crystals

MDPI

Review

Active and Programmable Metasurfaces with Semiconductor Materials and Devices

Can Cui, Junqing Ma, Kai Chen, Xinjie Wang, Tao Sun, Qingpu Wang, Xijian Zhang and Yifei Zhang *

Shandong Technology Center of Nanodevices and Integration, School of Microelectronics, Shandong University, Jinan 250100, China

* Correspondence: yifeizhang@sdu.edu.cn

Abstract: Active metasurfaces provide promising tunabilities to artificial meta−atoms with unnatural optical properties and have found important applications in dynamic cloaking, reconfigurable intelligent surfaces, etc. As the development of semiconductor technologies, electrically controlled metasurfaces with semiconductor materials and devices have become the most promising candidate for the dynamic and programmable applications due to the large modulation range, compact footprint, pixel−control capability, and small switching time. Here, a technical review of active and programmable metasurfaces is given in terms of semiconductors, which consists of metasurfaces with diodes, transistors, and newly rising semiconductor materials. Physical models, equivalent circuits, recent advances, and development trends are discussed collectively and critically. This review represents a broad introduction for readers just entering this interesting field and provides perspective and depth for those well−established.

Keywords: metasurface; active modulation; programmable metasurface; semiconductor materials; diodes; transistors

check for updates

Citation: Cui, C.; Ma, J.; Chen, K.; Wang, X.; Sun, T.; Wang, Q.; Zhang, X.; Zhang, Y. Active and Programmable Metasurfaces with Semiconductor Materials and Devices. *Crystals* **2023**, *13*, 279. https://doi.org/10.3390/cryst13020279

Academic Editor: Dmitri Donetski

Received: 16 December 2022
Revised: 31 January 2023
Accepted: 2 February 2023
Published: 6 February 2023

Copyright: © 2023 by the authors. Licensee MDPI, Basel, Switzerland. This article is an open access article distributed under the terms and conditions of the Creative Commons Attribution (CC BY) license (https://creativecommons.org/licenses/by/4.0/).

1. Introduction

Metasurfaces are two−dimensional metamaterials with strongly scattering subwavelength atoms, which can manipulate the properties of electromagnetic waves unnaturally and have unlocked many important applications [1–9], including clocking, flat lens, perfect absorption, optical computing, biosensing, etc. Typically, the optical properties of metasurfaces are set in stone post design due to their fixed spatial structures and material properties, which is referred to as "passive". Recently, various approaches have been frequently investigated to tune these passive metasurfaces. Mechanical means, such as deformable mirrors and elastic materials [10], can reconfigure the metasurface properties, however, which is typically limited by the system complexity and size as well as mechanical actuation accuracy. Alternatively, tunable metasurfaces can be achieved by integrating active components with pixelated metasurface architectures, which are well−known as active metasurfaces [4–6].

In recent years, active metasurfaces have gained concentrated interest from microwave to optical frequencies, enabling many promising applications, such as reconfigurable intelligent surfaces (RIS) in communication [11,12], tunable flat lenses in optics [13], and non−reciprocal devices in physics [14,15]. The active stimuli manipulate the amplitude, frequency, phase, and polarization states of electromagnetic waves dynamically, which typically requires electrical bias control [5,6]. In this regard, semiconductor−based control approaches are the most important candidate for active metasurfaces, particularly programmable and coding ones. With the development of semiconductor materials and fabrication technologies [2], semiconductor devices provide pixel−control capability due to their small footprint and friendly circuit integration and achieve small switching times down to several picoseconds due to the high electron mobility and high−speed structures. In addition, new semiconductors with high electron mobility and large−modulation

range, have high−frequency applications. While several review papers have discussed the developments and advances of active metasurfaces and metamaterials [4–6,10], this work approaches this hot topic from a distinct aspect of semiconductors, including the conventional devices, such as diodes and transistors, and newly rising materials with low dimensions. The diodes and transistors have been widely applied in active microwave circuits for decades [16], and were demonstrated as a beneficial method for digital coding and programmable metamaterials in the last few years [4,11,12]. On the other hand, new semiconductor materials bring in many interesting advances, such as high modulation speed and nonvolatility, and enable promising applications in new spectra, such as terahertz [17]. However, their material uniformity and bias control methods remain to be explored.

In this paper, we give a comprehensive review of the physical mechanisms of semiconductor materials and devices, design strategies combing both passive and active components, practical implementations, and emerging applications. First, microwave diodes including varactor, positive−intrinsic−negative (PIN), and Schottky diodes are discussed, whose equivalent circuit models are clear to experienced microwave engineers. Commercial packaged diodes bloom many exciting works at microwave frequencies and meet a significant frequency limit due to their dispersive electromagnetic properties and parasitic reactance. Next, transistors with two sets of control voltages are investigated, which can easily work at terahertz frequencies due to the advanced semiconductor materials and sophisticated foundry fabrication, such as high−electron−mobility transistors (HEMTs). However, the gate bias enhances the complexity of DC control networks. In addition, we present two−dimensional (2D) materials and phase change materials for active metasurfaces, which show little spectral threshold and provide good modulation capability from microwave to optical frequencies. Despite the current limits on material uniformity and pixel−control methods, these low−dimensional materials are promising candidates for future applications of active metasurfaces. We expect this review provides an interesting introduction for beginners and shows depth and perspective to the researchers in this realm from a different aspect.

2. Metasurfaces with Diodes

A diode is a two−terminal electronic device with asymmetric electrical conduction in different directions between two electrodes, which was founded by F. Braun in 1874 [18]. Typically, most diodes are made of silicon, but other semiconductors including III–V and the third generation semiconductors are also used. As the simplest electronic device, the diode has been applied to control microwave circuits for many decades, such as the varactor diode, PIN diode, and Schottky diode. Their typical structures and equivalent circuits are well−studied in the community of microwaves, as illustrated in Figure 1. With the benefit of commercial packages with high reliability, diodes are one of the most sophisticated and stable technologies for active and programmable metamaterials and RIS at microwave frequencies [6]. In addition, their simple electrode structures and bias networks are suitable for large arrays with complicated bias control.

2.1. Varactor Diodes

The varactor diode is a kind of positive–negative (p−n) diode that works under reverse bias voltage, as illustrated in Figure 1a, the p−n junction capacitance of which sweeps as the applied voltage changes [18]. Under a reverse bias, the built−in electric fields in the depletion region formed by the diffusion motion of the majority carriers are in the same direction as the applied electric fields. As the bias increases, the diffusion of the majority carriers becomes more difficult, the thickness of the depletion zone increases, and thus, the junction capacitance of the varactor diode decreases. Thus, its equivalent circuit is a voltage−controlled capacitor at microwave frequencies, as shown in Figure 1a, where parasitic inductor and resistor may need to be considered for precise simulation [11]. The commercially available varactor diodes packaged in Macom, Skyworks, etc., typically have

a large package size in millimeter scales and a working frequency lower than 60 GHz [16]. In this case, they have been widely used in tunable and reconfigurable metamaterials at microwave frequencies, enabling many important applications of radar, communication, sensing, and imaging systems [3,19–22].

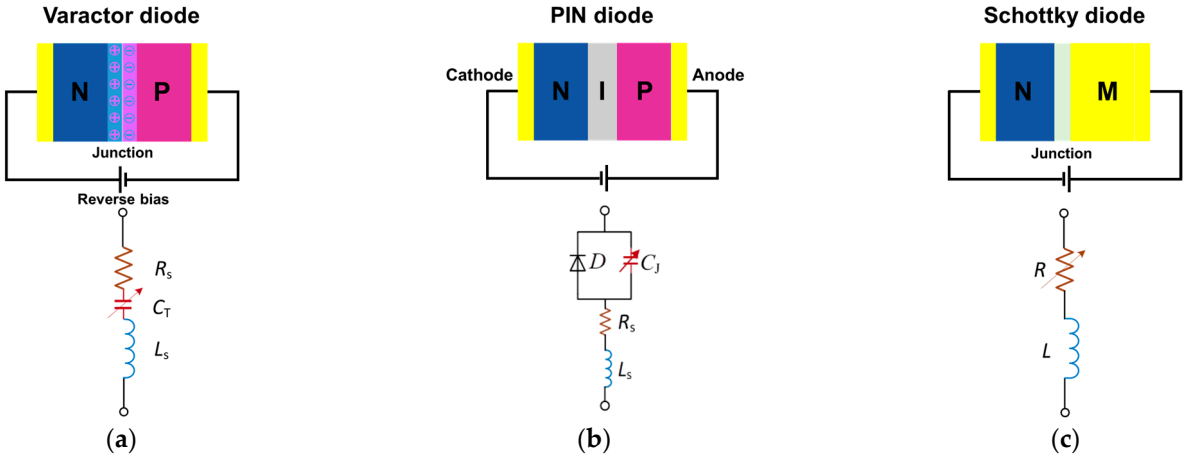

Figure 1. Schematics and equivalent circuits of various diodes. (**a**) Varactor diode. As a p−n diode under reverse bias, its equivalent circuit is a voltage−controlled capacitor. (**b**) PIN diode. Its equivalent circuit model is a tunable resistor. (**c**) Schottky diode. Its equivalent circuit model is a voltage−controlled resistor.

At the beginning of the twenty−first century, varactor diodes have been investigated to tune high−impedance surfaces for dynamic beam steering [23,24]. Later, a tunable metamaterial absorber was reported with varactor diodes and lumped resistors in 2007 [25]. The following works aim to achieve a large absorption rate and wide spectral tuning range, including electric−field coupled−LC (ELC) resonators [19], fishnet−like resonators [26], dual ELC resonators [27], spoof plasmonics [6], etc. In the last two years, varactor−controlled frequency selective surface (FSS) and electromagnetically induced transparency (EIT) structures have been reported with wideband frequency modulation [28,29], as shown in Figure 2a,b. The diodes are launched right on the effective coupling capacitor of the resonant structures. Several early reviews focus on active electromagnetic absorbers [30,31]. The readers may refer to them if they are interested. In addition to amplitude and frequency modulation, phase modulation of metasurfaces can be also achieved with varactor diodes [32].

Phase modulation function enables the well−known RIS. In 2014, the first digital and programmable metamaterials were proposed by T. J. Cui and his colleagues, whose unit cells possess either 0 (0 state) or π (1 state) phase responses with digitally controlled diodes [33]. The coding sequence for 0 or 1 state can be programmed by field−programmable gate array (FPGA) hardware, and different sequences achieve various far−field reflection patterns on a single active metasurface. In 2015, Y. Li et al. reported a transmission−type programmable metasurface with varactor diodes in a two−layer binary coding unit. The rows and columns of the metasurface can be controlled simultaneously with binary coding [34]. A reprogrammable hologram was realized by switching the phase states of coding metasurface with varactor diodes in 2017 [35]. The resonant metasurfaces show abrupt phase change at the resonant frequency, and large−phase modulation can be obtained by a sweeping frequency. The beam pattern of a whole metasurface can be digitally coded as the following equation

$$f(\theta,\varphi) = \sum_{q=1}^{N}\sum_{p=1}^{M} E_{pq}(\theta,\varphi) exp\left\{ j\frac{2\pi}{\lambda_c}\left[(p-1)d_x \sin\theta\cos\varphi + (q-1)d_y \sin\theta\sin\varphi\right]\right\}, \quad (1)$$

where E_{pq} (θ, φ) is the far−field pattern pertaining to the (p, q)th coding element computed at the resonant frequency f_c, θ and φ are the elevation and azimuth angles, respectively, d_x

and d_y are the element periods along the X− and Y−directions, respectively, and λ_c is the wavelength of the central frequency [36]. In 2020, an optically driven digital metasurface was reported to avoid the complex electric bias networks, as illustrated in Figure 2c, where a large−phase modulation from 0 to 180° is obtained on two hollow metal patches bridged with a varactor diode [11]. In 2020, the dynamic vortex beam has been generated digitally by using varactor−based metasurfaces through FPGA control [12].

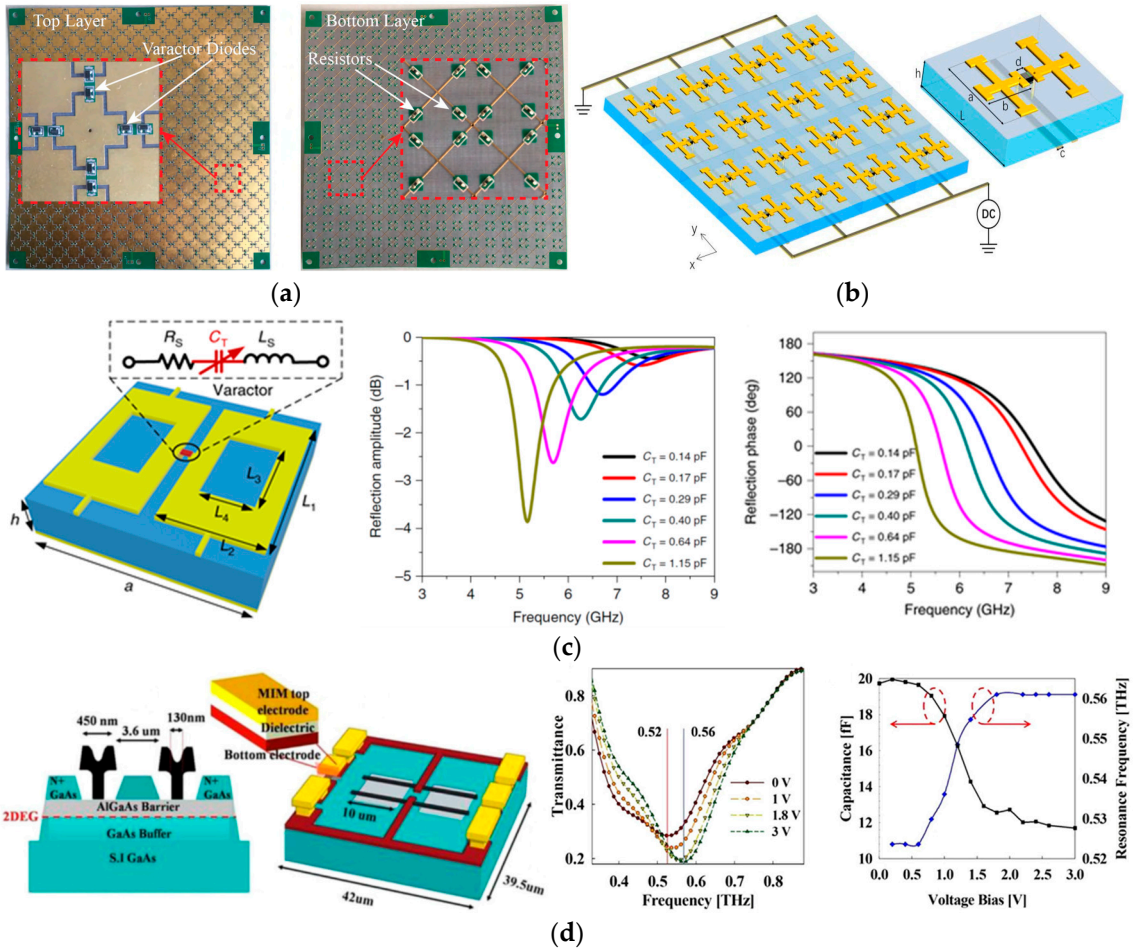

Figure 2. Active and programmable metasurfaces with varactor diodes. Frequency modulation of (**a**) FSS [28] and (**b**) EIT structures [29]. The varactor diodes change the coupling capacitance of the metasurfaces. (**c**) Hollow patch RIS with varactor diodes [11]. The diode actively modulates the reflection phase by sweeping the resonant frequency, where the metasurface shows abrupt phase change. Copyright Nature, 2020. (**d**) Terahertz metasurface modulated with MSM varactors [37]. The high−frequency MSM structure is a combination of two Schottky capacitors on the top of AlGaAs/InGaAs/GaAs double heterostructure.

In sum, varactor diodes are beneficial for the frequency and phase modulation of metasurfaces and enable resonant−type RIS by tuning its resonant frequency. However, the commercially available varactor diodes with large package sizes cannot work at terahertz frequencies, i.e., above 100 GHz. Metal–semiconductor–metal (MSM) device with varactor functionalities was demonstrated to modulate the resonant frequency of SRR metasurfaces from 0.52 to 0.56 THz [37]. This device is similar to two Schottky diodes joined together, whose capacitance is determined by the depletion region of the Schottky junction, as shown in Figure 2d. Its shortcoming is the more complicated and expensive semiconductor fabrication.

2.2. PIN Diodes

The PIN diode is composed of a layer of p−type semiconductor, a layer of intrinsic semiconductor with low doping, and a layer of n−type semiconductor, as illustrated in Figure 1b. Figure 1b also illustrates the equivalent circuit model of a PIN diode for on/off switching. The resistivity of the intrinsic area is low when a forward bias is applied, which is the on the state. The diode resistance decreases as the forward bias increases. With reverse bias, it shows high resistance, which corresponds to the off state [38]. In contrast to the varactor diodes, the PIN diodes are voltage−controlled resistors with parasitic capacitors (typically for the off−state) and inductors. Currently, commercially available PIN diodes have similar millimeter−scale package sizes as the varactor diodes and typically operate below 100 GHz [16]. Before active metasurfaces, they have been widely used in circuit switches, digital phase−shift circuits, and phased array antennas at microwave frequencies [16,39–41].

Using PIN diode to tune FSS structures can be found in the early 1990s [42,43], which is even before the concept of metamaterials was proposed. Firstly, switching between transmitting and reflecting states with PIN diode−based FSS structures has been reported in many papers in the antenna community [44–46]. Later, research interest diverged into incident angle tuning [47], reflection modulation [48], and bandpass shaping [49]. The equivalent circuit model of active FSS with PIN diodes was well discussed in [50]. In 2011, A. R. Katko et al. reported a radio frequency (RF) limiter metamaterial with a maximum isolation of 9.3 dB and a broad bandwidth of 18% by using PIN diodes [51]. In 2017, EIT structures were significantly modulated by using PIN diodes, which locate in the gap of the wire pair for continuous control of wave transmission [52], as shown in Figure 3a. Today, active metasurfaces modulated with PIN diodes have still gained considerable attention, such as nearly perfect reflection and transmission [53,54] ultra−wideband absorption [55,56], see Figure 3b, and ultra−wideband polarization conversion [57]. The fantastic function of switching between transmitting and absorbing states shows great potential in electromagnetic stealth and electromagnetic compatibility (EMC), inspiring many interesting applications of the active or reconfigurable antenna and radome [55,58,59]. In addition, wearable antenna with PIN−controlled metasurfaces has been investigated for medical applications on flexible substrates [60].

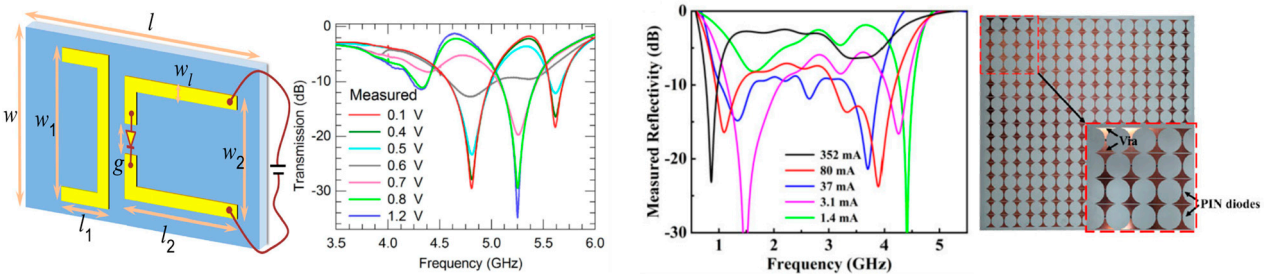

(**a**) (**b**)

Figure 3. *Cont.*

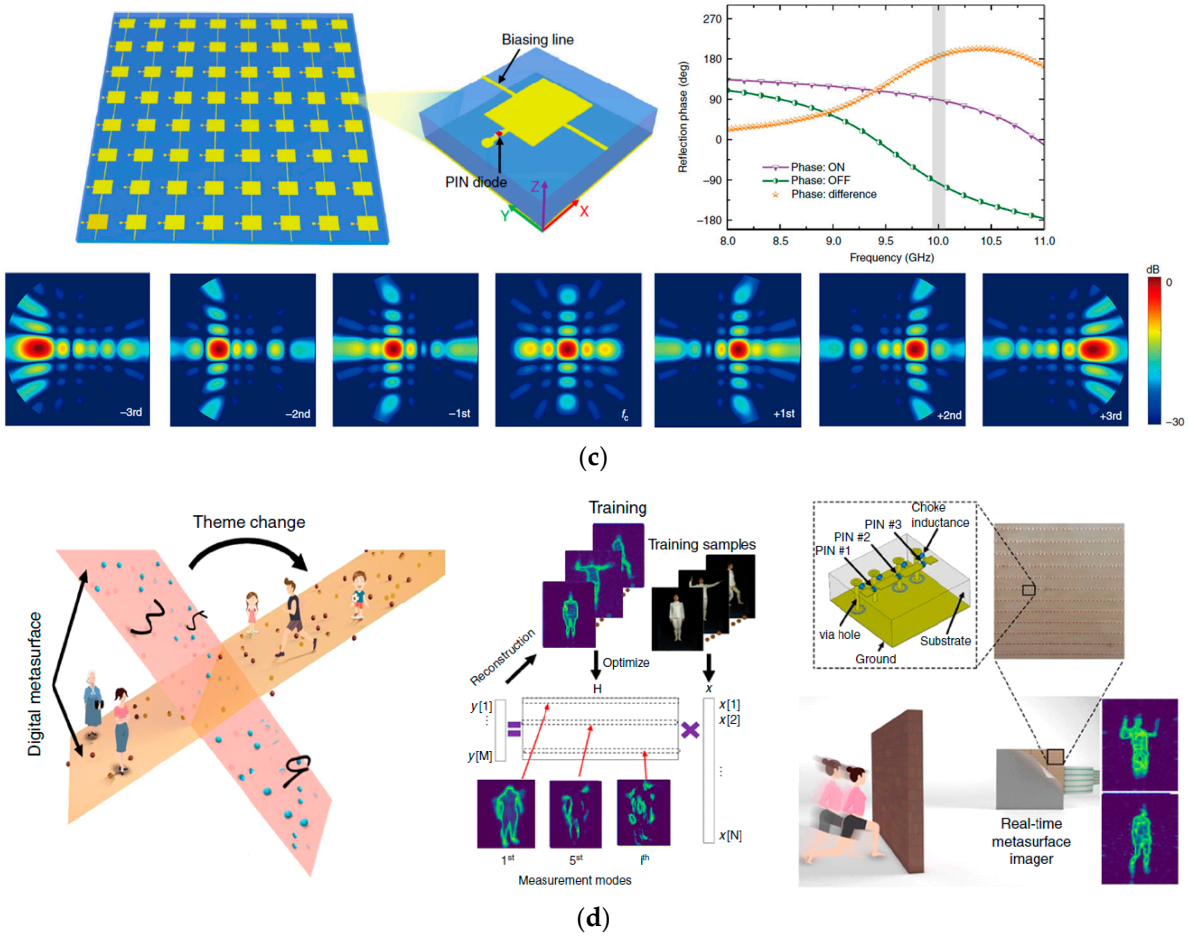

Figure 3. Active and programmable metasurfaces with PIN diodes. (**a**) Amplitude modulation of EIT with PIN diode [52]. (**b**) Ultra−wideband absorber achieving continuous amplitude modulation with PIN diodes [56]. (**c**) Space−time−coded metasurfaces with PIN diodes [36]. The diode can sweep the reflection phase between on and off states and implements the harmonic beam steering. (**d**) Machine−learning reprogrammable metasurface imager with PIN diodes [39].

Currently, the PIN diode is also one of the most mature and stable technologies for RIS applications. Similar to varactor diodes, PIN diodes can be integrated into each metasurface pixel with subwavelength scales. Combined with the multi−layer−printed circuit board (PCB) power supply networks, each pixel can be coded individually and digitally in quantized phase states and programmed to constitute RIS with complex functions [28,33]. In 2018, L. Zhang et al. expanded the space−coded RIS configuration to space−time−coded RIS configuration with PIN diodes, which manipulate microwaves in both space and frequency domains [36]. Figure 3c illustrates the space−time−coded digital metasurface and its harmonic beam steering at optimized space−time coding sequences. In 2019, a reprogrammable metasurface imager was demonstrated by using multiple PIN diodes to produce phase differences [39], as shown in Figure 3d. Real−time imaging was obtained with machine−learning technologies. Later, PIN diode−based metasurface have been proposed to transmit digital information directly in 2021, which is a completely new architecture for wireless communications without using complicated digital–analog convertor and a series of active/passive microwave devices [40]. Frequency division/space division multiplexing wireless communication was demonstrated with PIN diodes by using digital coding to control the active phase states, realizing signal transmission at different access terminals at the same time with a transmission rate of 2.5 Mbps at 9.5 GHz [12]. The above−mentioned coding and programmable metasurfaces only achieve half−space modulation, i.e., reflection−type modulation. In 2021, full−space control of the programmable

metasurface was reported by L. Bao and his colleagues, in which reflection and transmission share the same metasurface aperture [61]. The unit pixel of the full−space metasurfaces is controlled by using three PIN diodes with different bias sequences.

However, the working frequency of the active metasurfaces modulated with PIN diodes is limited by the highest operating frequency of the PIN diode itself. For the commercial−packaged PIN diodes, their switching performance is affected by the parasitic reactance dispersedly, so they usually operate below terahertz frequencies [16]. Recent research shows that the diode performance may be improved by designing compensation structures or using new materials. In 2020, A. Singh et al. reported that the highest working frequency of a PIN single−pole–single−throw (SPST) switch can be doubled from 6 GHz (the limit frequency that the manufacturer states) to 10.55 GHz with an isolation range of 40.9 dB [62]. This method may be used to reduce the influence of parasitic reactance at millimeter wave frequencies. On the other hand, L. Liu and her colleagues designed a heterojunction AIGaAs/GaAs PIN diode at the Ka−band, which shows good potential in the applications of terahertz switches [63].

2.3. Schottky Diodes

Differing from the classical p−n or PIN diode, the Schottky diode is formed by a metal–semiconductor junction, which typically has a low forward voltage drop and a very high switching speed [64]. Typically, the n−type semiconductor has a much higher electron concentration than the metal, so electrons move from semiconductor to metal by diffusion. When the diffusion and drift motion of electrons reach a balance, a Schottky barrier is formed [65]. Since Schottky diodes only use electrons as carriers without any accumulation of minority carriers, they have a small loss and switching time and can operate at high frequencies, including the terahertz range. Figure 1c illustrates a typical Schottky diode and its equivalent circuit at microwave frequencies. Similarly, a Schottky diode or Schottky junction can be described as a voltage−controlled resistor with smaller reactance with respect to the PIN diode. In addition, Schottky diodes have been widely used as high−frequency detectors and mixers in the front−end transmitters and receivers at millimeter−wave and terahertz frequencies [66–70].

In 2006, H.−T. Chen and his colleagues proposed active terahertz metamaterial devices with ELC resonators and Schottky diodes on an n−type GaAs substrate [71]. Distinguishing from the aforementioned varactor and PIN diodes, the Schottky contact is shared by both RF electrodes, and another ohmic electrode provides a DC bias for junction control, which means that only the Schottky junction contributes to the active modulation. Then, people demonstrated an SRR−based phase modulator with a similar diode configuration at 1 THz [72]. Later, extraordinary transmission (EOT) through subwavelength metal holes was electronically modulated with GaAs Schottky junctions [73]. In 2021, X. Liu and his colleagues reported ultra−broadband terahertz modulation with periodic metal lines and Schottky junctions, whose modulation speed is around 100 kHz [74]. In addition to the III−V semiconductors with high electron mobility, Y. Zhang et al. designed active surface plasmon polariton (SPP) metamaterials with In−Ga−Zn−O (IGZO) Schottky junctions at millimeter−wave frequencies in 2019, which shows significant modulation depth [75], as shown in Figure 4a. IGZO is an amorphous oxide semiconductor with a typical electron mobility was less than 50 $cm^2/(V{\cdot}s)$, which is suitable for flexible and wearable electronics. Later, multi−frequency, multi−bit control of SRRs has been demonstrated with IGZO Schottky structures [76]. In 2021, active THz metamaterials with IGZO Schottky junctions was demonstrated at 400 GHz, which is approximately 100 times higher than the on/off speeds of the IGZO Schottky diode [77], see Figure 4b. This junction configuration addresses good high−frequency capabilities without considering the electron transfer between the cathode and anode of the diodes.

As a high−speed rectifying diode, the Schottky diode also can be directly used to control metamaterials with a similar configuration as the PIN diode. In 2020, R. Phon and S. Lim reported a power−level modulated metamaterial with the Schottky diode, which is

mounted on the central slit of the device [78]. The metamaterial functions as a bandpass filter or a reflector at low and high power levels, respectively, as shown in Figure 4c. In 2021, air−bridged Schottky diodes were integrated into a metamaterial circuit for phase shifting at millimeter wave frequencies [79]. A maximum phase shift of 195° can be achieved at around 41.5 GHz. In 2020, Y. Zhou et al. reported a bidirectional Fano resonance switch in plasma metamaterials by switching the Schottky diode under forward and reverse bias voltages [80], as illustrated in Figure 4d.

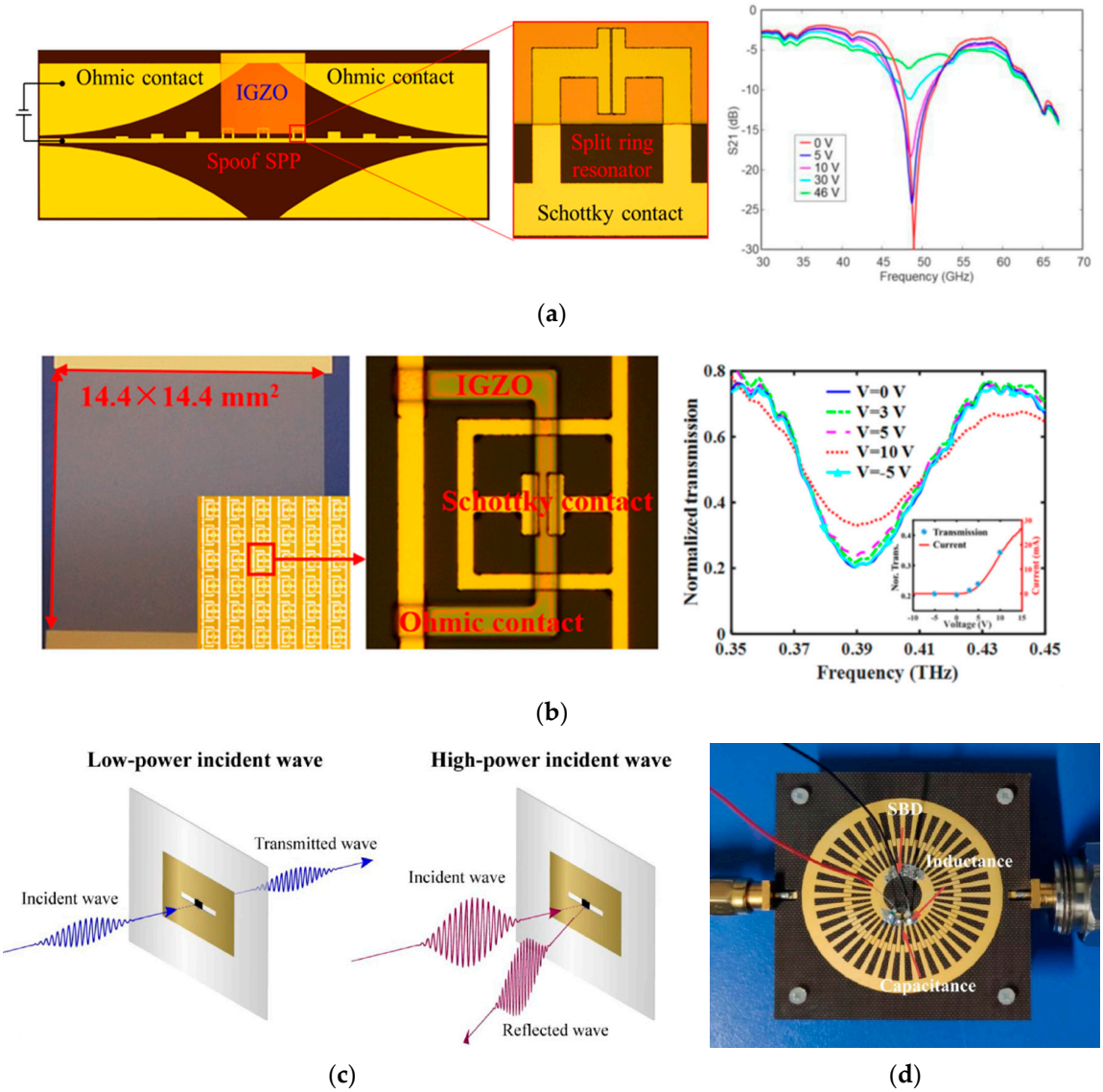

Figure 4. Active metasurfaces with Schottky junctions and diodes. Copyright American Chemical Society, 2019. (**a**) Amplitude modulation of surface plasmon polariton metamaterials with IGZO Schottky junctions [75]. (**b**) Active terahertz metamaterials with IGZO Schottky junction at 400 GHz [77]. (**c**) Power−level controlled metamaterial structures with Schottky diodes [78]. (**d**) Plasmonic metamaterials with Schottky diode switch [80].

The working frequency of Schottky diodes is continuously improved as the development of semiconductor materials and fabrication technologies [66–70,81–83]. Schottky diode mixer on GaAs substrate was reported at 1.098 THz in 2019 [69], and phosphating steel Schottky diode with T−shape contact achieved a cut−off frequency of up to 9 THz in 2022 [70]. These exciting works make Schottky diodes promising for terahertz applications, although the working frequency of the aforementioned metasurfaces with Schottky

diodes is lower than the intrinsic cut−off frequency of the Schottky diode itself. One disadvantage of advanced Schottky diodes is the fabrication difficulties and high cost due to nanometer−scale metal air bridges [64]. We expect more works on Schottky−functioned active and programmable metasurfaces in the next few years.

3. Transistor Based Metasurfaces

The transistors are a kind of three−terminal solid semiconductor devices with many important functions [84], such as amplification [85], switching [86], and signal modulation [87], which typically include bipolar junction transistors (BJTs) and field−effect transistors (FETs) at high frequencies. To actively modulate metasurfaces, the transistors typically functioned as a switch controlled by the gate bias [16,84]. Figure 5a illustrates a typical configuration of a HEMT and its equivalent circuit model, where the two−dimensional electron gas (2DEG) channel can be switched between on and off states. It can be seen that the circuit model of a transistor is more complicated than the diodes. The key circuit element of the channel is a voltage−controlled resistor with parasitic reactance.

Due to the short channel length, transistors have been seldom applied for active metasurfaces at microwave frequencies. In 2017, A. Li et al. reported a tunable high−power surface wave absorber on a multilayer PCB substrate with soldered transistors at 2.4 GHz, achieving a sharp absorption response [88]. The gate bias provides an additional degree of freedom for absorption control at a cost of an additional circuit layer. In contrast, semiconductor FETs (particularly HEMTs) have gained considerable attention in the terahertz realm. In 2011, D. Shrekenhamer and his colleagues designed a terahertz modulator based on metamaterials and HEMTs on GaAs substrate, whose modulation speed is as high as 10 MHz due to the high mobility of 2DEG [87]. Later, gallium nitride (GaN) HEMT pushes the modulation speed up to a GHz range on a composite metamaterial with a double−channel heterostructure [89,90], as illustrated in Figure 5b. In 2021, W. Pan and his colleagues reported active metasurfaces on silicon carbide (SiC) substrates with HEMTs at 0.22 and 0.34 THz [91]. The resonances at different frequencies can be independently modulated by using two HEMTs in each metasurface pixel. In addition to the GaAs or GaN HEMTs, other semiconductors and transistors have also been investigated for this application. In 2015, F. Ren and her colleagues proposed a hybrid metamaterial based on the IGZO thin−film transistor (TFT) array, whose resonant mode is modulated at 0.76 THz by changing the conductivity of the transparent oxide layer [92]. Later, W. Xu et al. designed an active metamaterial device with amorphous−IGZO TFTs at 0.75 THz [93]. Its absolute modulation range is less than one percent with a bias voltage up to 24 V, as shown in Figure 5c. Silicon is another promising choice due to the sophisticated fabrication technologies and multilayer circuits. In 2017, a terahertz absorber with CMOS transistors was reported in [94]. In 2021, active SRRs fabricated with CMOS technologies were reported with frequency modulation capabilities [95].

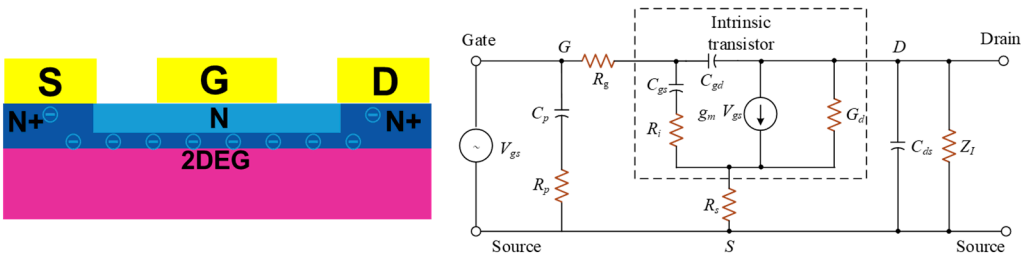

(**a**)

Figure 5. *Cont.*

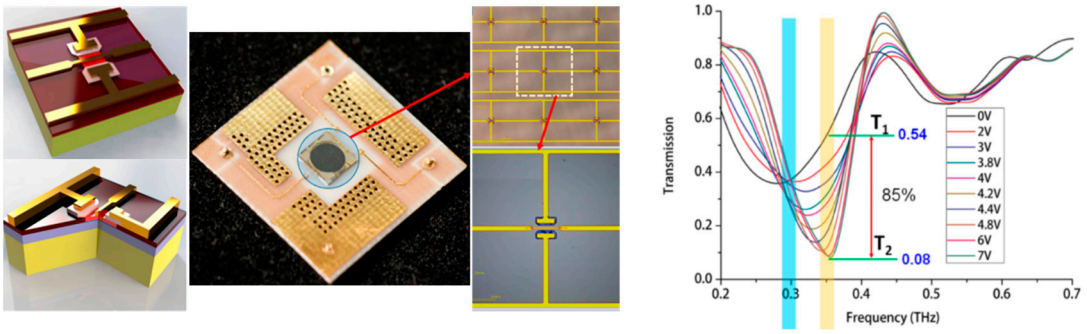

(**b**)

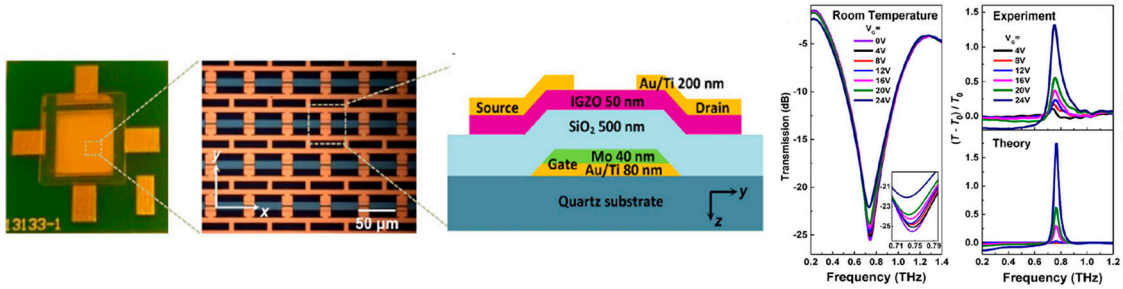

(**c**)

Figure 5. Active metasurfaces with FETs. (**a**) Configuration of a HEMT and its equivalent circuit model. (**b**) Terahertz metasurfaces modulated with HEMTs on GaN substrate [89]. Its modulation speed is up to 1 GHz. Copyright American Chemical Society, 2015. (**c**) IGZO TFT−based metasurfaces at 0.75 THz [93].

Differing from the diodes, transistors are more suitable for terahertz metasurfaces due to the mature semiconductor fabrication technologies with high precision and compact integration. Among the above semiconductors, GaAs and GaN address advances in high frequency and high speed, silicon may be suitable for RIS applications due to the multilayer circuits in CMOS fabrication, and oxide semiconductor shows good flexibility and low cost. However, their gate electrode makes the design of the bias network more complex, which may also induce mutual coupling in the subwavelength scales.

4. Active Metasurfaces with Two−Dimensional Materials

In addition to the relatively bulky semiconductors, 2D materials have gained a great interest in active metasurfaces recently due to their promising electric, optical, thermal, and mechanical properties [96–98]. Two−dimensional materials consisting of a single layer of atoms, such as graphene [99–101], HBN [102], MoS_2 [103], WS_2 [104], etc., may achieve high carrier mobility and tunable band gap and thus show great modulation capability from microwave to optical frequencies. The topic of 2D materials is too broad to cover in limited pages. To focus our scope on active metamaterials, we will mainly discuss graphene in this section, which to our knowledge is the most widely used two−dimensional material for active metamaterials. Regarding the other kinds of 2D materials, please refer to [17,105] for your interest.

Graphene, a crystalline allotrope of carbon atoms in a 2D honeycomb lattice, is the first kind of 2D material, the strongest material known, and a superb conductor of both heat and electricity [106]. In addition, graphene is a promising candidate for flexible

applications [107–110]. The conductivity of graphene is theoretically determined by the Kubo formula as

$$\begin{aligned}\sigma(\omega,\Gamma,\mu_c,T) &= \sigma_{intra}(\omega,\Gamma,\mu_c,T)+\sigma_{inter}(\omega,\Gamma,\mu_c,T)\\ \sigma_{intra}(\omega,\Gamma,\mu_c,T) &= \frac{-je^2k_BT}{\pi\hbar^2(\omega-j2\Gamma)}\left[\frac{\mu_c}{k_BT}+2ln\left(exp\left(\frac{\mu_c}{2k_BT}\right)+1\right)\right],\\ \sigma_{g,inter}(\omega,\Gamma,\mu_c,T) &= \frac{-je^2}{4\pi\hbar}ln\left(\frac{2|\mu_c|-(\omega-j2\Gamma)\hbar}{2|\mu_c|+(\omega-j2\Gamma)\hbar}\right),\end{aligned} \tag{2}$$

where ω, e, Γ, μ_c, T, k_B, and $\hbar$ are the angular frequency, the charge of the electron, dispersion rate, chemical potential, temperature, Boltzmann's constant, and reduced Plank's constant, respectively [105]. It can be seen that the complex conductivity of graphene is tuned by the chemical potential, which can be controlled by the applied gate bias, as shown in Figure 6a. The interband term dominates in the visible and near−infrared range, and the intraband term dominates at far−infrared frequencies and below. In an ideal case, graphene conductivity shows a larger modulation range at microwave and terahertz frequencies than at optical frequencies. Figure 6b illustrates the typical gate configurations for sweeping the chemical potential, i.e., top gate, bottom gate, and electric double−layer capacitor (EDLC) [97]. Top gate and bottom gate configurations are commonly used for TFTs, which is similar to the gate configuration in Figure 5a. Due to the chemical doping, the Dirac point of graphene is typically not right at 0 V. In this case, the gate dielectric should be as thin as possible to reduce the applied gate voltage. In contrast, ion gel or liquid forms an EDLC for gating graphene, which is more adaptive than the top and bottom gates. However, the graphene modulation speed is limited by the moving speed of ions in EDLC, and the dielectric constant of ion gel and liquid needs to be considered for the accurate design of metasurfaces. To improve the modulation capability, another graphene layer can be used to replace the ground electrode in EDLC, as shown in Figure 6c. The modulation response time is around 0.3 s [111].

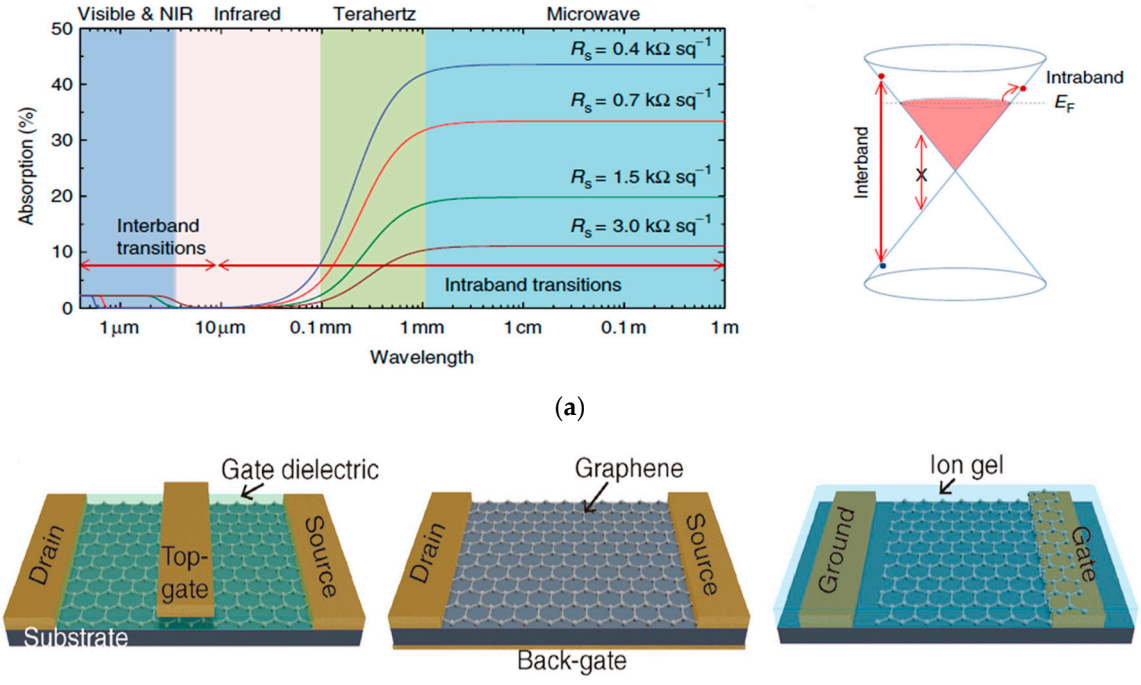

Figure 6. *Cont.*

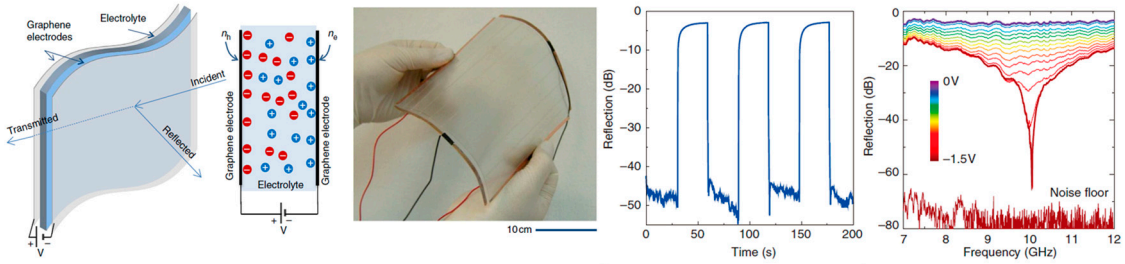

(**c**)

Figure 6. Tunable electromagnetic properties and gate configurations of graphene. (**a**) Calculated spectral absorption of single−layer graphene with various sheet resistance from microwave to visible frequencies and the corresponding electronic band structure [111]. (**b**) Conventional gate configurations for graphene, including top gate, bottom gate, and EDLC [97]. Copyright John Wiley and Sons, 2020. (**c**) Adaptive microwave absorber with two graphene electrodes sandwiching ion liquid [111]. The modulation band is from 7 to 12 GHz, and the response time of modulation is around 0.3 s.

Since graphene was founded in 2004 [110], it has been investigated for modulation devices from microwave to visible frequencies based on its sweeping conductivity [111,112]. In 2011, L. Ju et al. reported graphene plasmonic metamaterials with micro−ribbon arrays, which can be tuned over a broad terahertz range by changing the chemical potential [113]. In 2012, a metal−graphene hybrid metasurface was demonstrated with amplitude and phase modulation at terahertz frequencies [114]. The characterized modulation speed is 100 kHz. Later, graphene metasurfaces and metal–graphene hybrid metasurfaces gained considerable attention. Many adaptive absorbers with graphene have been reported, revealing a high absorption rate and broad bandwidth [115–119]. In 2021, J. Zhang et al. proposed a graphene−based optically transparent and flexible metasurface, whose absorption rate is up to 90% from 7 to 18 GHz [98], as shown in Figure 7a. Frequency modulation of graphene−based hybrid metamaterials and all−dielectric metamaterials was reported in [120–123]. In 2022, M. Feng et al. reported active hybrid surface plasmon polaritons, whose cut−off frequency and slow−wave phase are significantly modulated by using graphene grooves [123], as illustrated in Figure 7b. Modulation speed is another big concern for graphene modulation. In 2015, hybrid SRRs with graphene surface plasmons achieved a modulation depth of 60% and a modulation speed of 40 MHz [124]. Later, Hybrid graphene metasurfaces for mid−infrared light modulation were reported by B. Zeng and his colleagues [96], as shown in Figure 7c. The characterized modulation depth is as large as 90%, and the modulation speed exceeds 1 GHz. In 2021, G. Choi et al. reported a graphene−based active metasurface with a modulation speed of up to 500 GHz [125].

Furthermore, active metasurfaces with graphene have been investigated for various wireless applications. The hybrid metasurfaces in Figure 7c have been used for single−pixel imaging in the mid−infrared range in 2018 [96]. In addition to imaging, graphene metamaterials can be used to improve the performance of antennas and reconfigure antenna properties, such as radiation patterns, polarization states, and beam steering angles [126–129]. In addition, graphene metasurfaces have been proposed for binary coding. In 2021, Y. Gong and his colleagues simulated metal–graphene metasurfaces with two resonances at 0.85 and 1.14 THz modulated individually [130], which enables 00, 01, 10, and 11 coding, as shown in Figure 7d.

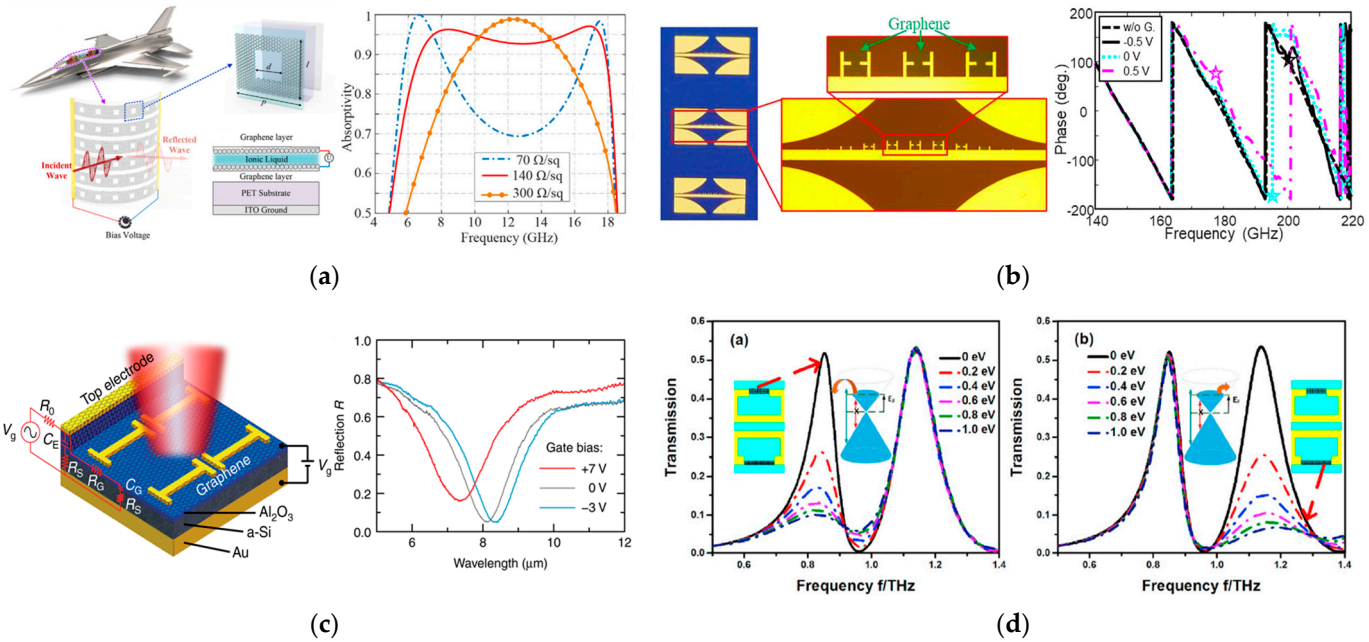

Figure 7. Active and programmable metasurfaces modulated with graphene. (**a**) Graphene metamaterial with adaptive absorption on transparent and flexible substrate at microwave frequencies [98]. Copyright Elsevier, 2021. (**b**) Hybrid surface plasmon polaritons with phase and frequency modulation controlled by graphene [123]. (**c**) Hybrid graphene metasurfaces for mid−infrared light modulation. Its modulation speed is as high as 1 GHz [96]. (**d**) Binary coding graphene−metal hybrid surface at terahertz frequencies [130]. Copyright Elsevier, 2021.

Although graphene−based metasurfaces address high modulation speeds up to 1.83 ps and are a good promise in wireless systems [125–129], material uniformity is a big problem to solve, which is fatal for microwave metasurfaces with large dimensions. Various transfer technologies have been developed to improve the graphene quality, such as paraffin−assisted transfer [131]. Another concern is how to control the pixel of graphene metasurfaces independently, which inhibits the applications of programmable metasurfaces and RIS.

5. Phase Change Materials Metasurfaces

Phase change materials (PCMs) are a kind of substance that release and absorb heat energy when their phase changes, which is typically called the latent heat of the phase transition [132]. The electronic and optical properties of PCMs, such as germanium−antimony−tellurium (GST) [133], vanadium dioxide (VO_2) [134], and gallium (Ga) [135], change drastically under an amorphous−crystalline phase transition, which enables unity−scale index changes for active metamaterials. Therefore, PCMs have been considered a promising candidate to develop reconfigurable metasurfaces [10,136]. Their phase transition characteristics can be controlled quickly with temperature, current, and light, and their modulation may be non−volatile [136–138].

5.1. Vanadium Dioxide

VO_2 is a kind of PCM widely used in the terahertz realm, whose phase transition temperature is typically around 68 °C [136]. It has a monoclinic crystal structure below this temperature and a tetragonal structure above this temperature, which corresponds to an insulator−to−metal phase transition at the phase transition temperature [139], as illustrated in Figure 8a. During the phase transition, the conductivity of VO_2 may vary several orders of magnitude under thermal heating, electrical biasing, and optical excitation. Typically, the thickness of VO_2 films is less than 200 nm, i.e., much smaller than the wavelength, so these films are somewhat transparent even in the metallic state [140].

Due to the large conductivity variation, VO_2 has been applied in the applications of active metasurfaces in the microwave, terahertz, and infrared regions [10,136]. The most fundamental phase−transition mechanism is thermal heating, which is typically stable and simple, but neither fast nor precise. Early in 2010, M. Seo et al. reported active terahertz nanoantennas with VO_2, achieving an ultra−broad bandwidth and a huge extinction ratio of over 10,000 [140]. Later, EOT in λ/100,000 nanogaps was modulated with VO_2 film [141], and an ultrathin quarter−wave plate controlled with VO_2 was reported in [142]. In 2018, S. Wang et al. reported a chiral metamaterial with periodic circular holes and VO_2 film, which controls the circular dichroism or polarization rotation of terahertz waves [143], as shown in Figure 8b. In addition to thermal heating, electrical bias is another convenient choice with fast switching speed down to nanoseconds. In 2011, Y.−G. Jeong et al. represented the slot antenna array fabricated on a thin VO_2 film with a 98% modulation range for the wave transmission [144]. Later, scattering−based modulation has been demonstrated in the bowtie antenna array connected with the wire grid [145], as depicted in Figure 8c. Optical excitation can switch the phase states of VO_2 in ultrafast response time without using any bias lines [146], see Figure 8d. However, due to the small film thickness, plasmonic structures may be desired to enhance the optical pump [136]. Regarding the modulation functions, amplitude modulation of transmission and reflection have been reported in [137,138,147–150], and frequency and phase modulation have been investigated in [150–157] in the past three years.

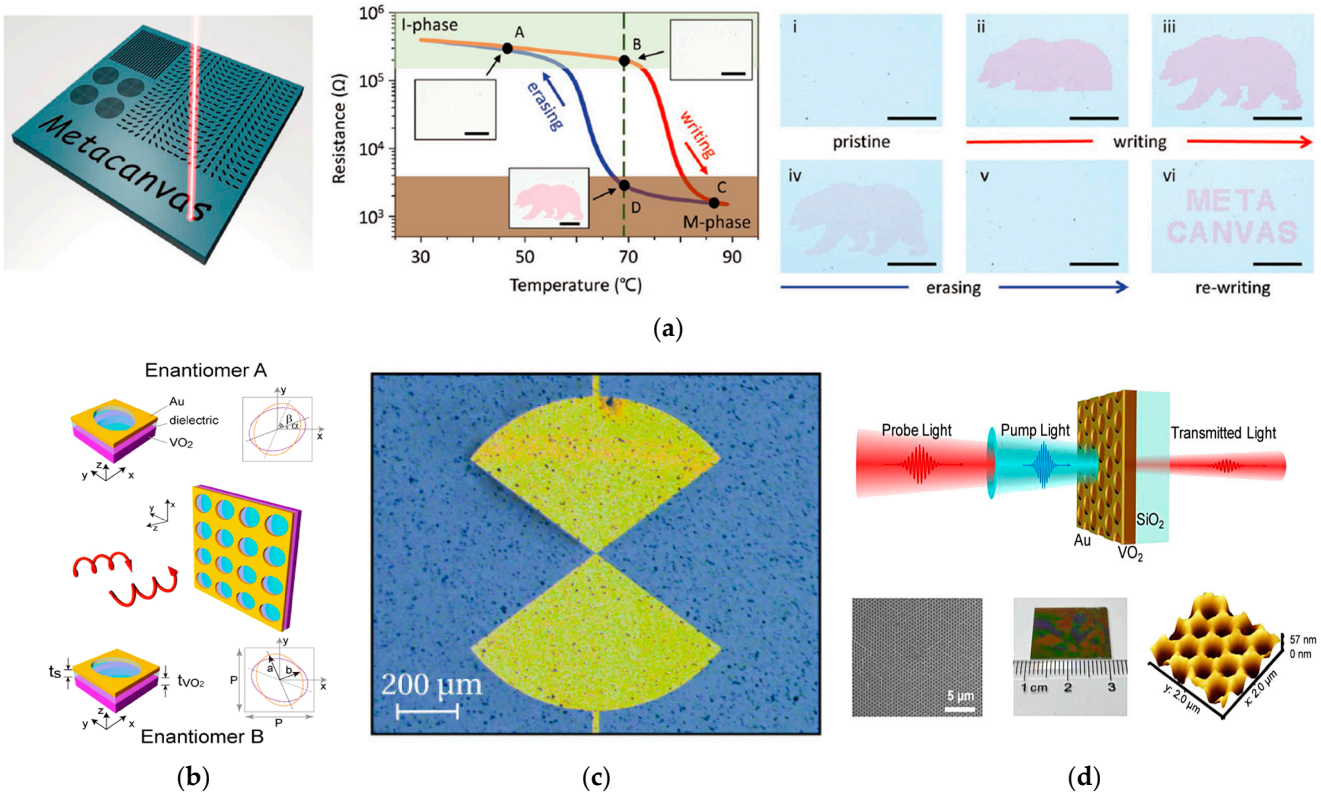

Figure 8. *Cont.*

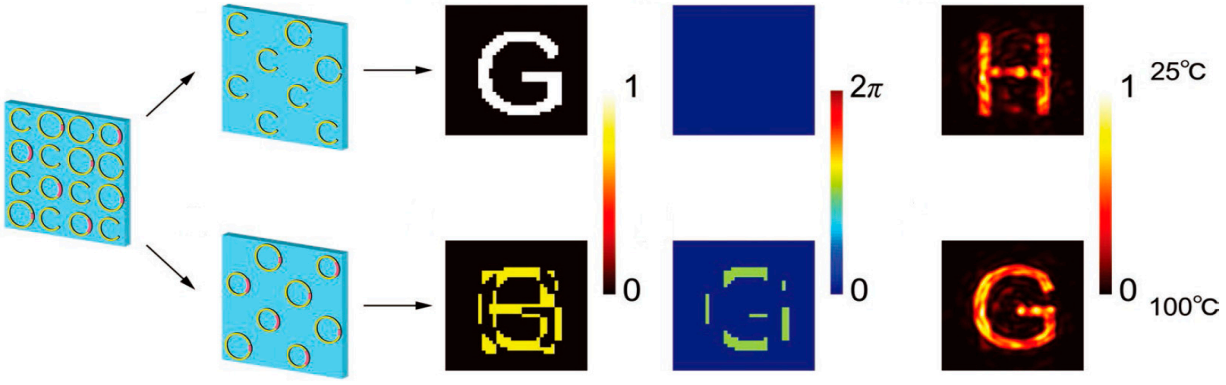

(**e**)

Figure 8. Dynamic metasurfaces with VO_2. (**a**) A rewritable canvas with laser−controlled metasurfaces [139]. The resistance of VO_2 sweeps as the temperature changes. Copyright John Wiley and Sons, 2018. (**b**) Thermally controlled chiral metasurfaces [143]. (**c**) Electrically controlled nanoantenna arrays with wire grid [145]. (**d**) Optically controlled metasurfaces for amplitude and frequency manipulation [146]. (**e**) Active SRR metasurfaces integrated with VO_2 for holography imaging [153]. Copyright John Wiley and Sons, 2019.

Active metasurfaces with VO_2 have found many important applications, such as holography and beamforming. Programmable metasurfaces have been demonstrated for independent manipulation of dual−polarized terahertz waves with VO_2 microwires [158], beam scattering patterns with VO_2 cut−wires [159], and wavefront and polarization state with C−shaped metal−VO_2 hybrid resonators [160]. In 2019, holographic imaging has been demonstrated by using VO_2−based metasurfaces with temperature control [153], as illustrated in Figure 8e.

5.2. Chalcogenides

Telluride−based chalcogenide materials show non−volatile and reversible phase change between crystalline and amorphous states, such as germanium tellurium (GT) and germanium antimony tellurium (GST), which have been widely investigated for active metasurfaces at microwave and infrared frequencies [10,136]. The crystalline and amorphous states address significant differences in electrical and optical properties, such as conductivity and permittivity. The temperature−dependent resistivities of GT, $Ge_2Sb_2Te_5$, $Ge_2Sb_2Se_2Te_3$, and $Ge_2Sb_2Se_4Te_1$ are reported in [161,162], respectively, as illustrated in Figure 9a,b. The amorphous state transfers to the crystalline state at the crystallization temperature, and the crystalline state gets disordered at the melting temperature [163]. This unique phenomenon enables the commercial application of non−volatile electronic data storage, such as Intel's Optane^{TM} memories. In addition, optical memories can function in a similar way by using optical pulses [136].

Active metasurfaces with chalcogenide materials have gained considerable interest in recent years. In 2015, Q. Wang et al. reported phase−change canvas, lens, and multiplexing devices with $Ge_2Sb_2Te_5$ [164], and C. H. Kodama et al. demonstrated tunable SRRs using GT [165]. Nonvolatile switchable metamaterials operating in the ultraviolet to the high−energy visible spectral range were reported for the first time in 2019 [166]. In the same year, P. Pitchappa et al. proposed a $Ge_2Sb_2Te_5$−integrated terahertz metamaterial switching with spatial and temporal selectivity [167], as shown in Figure 9d. A reconfigurable all−dielectric metalens was reported with a large phase modulation range of 2π and diffraction−limited performance in [13], achieving tunable focal length, see Figure 9c. In 2022, thermally switchable bi−functional metasurfaces with $Ge_2Sb_2Te_5$ achieve broadband polarization conversion and absorption [168], as illustrated in Figure 9e. The polarization conversion ratio is larger than 90% from 0.6 to 1.15 THz. Figure 9f shows conjugated bilayer chiral metamaterials integrated with $Ge_2Sb_2Te_5$, revealing an ellipticity

modulation of ~36° and a polarization plane rotation of ~32° at 0.73 THz [169]. Coding and programmable metasurfaces with GT materials have been reported with reconfigurable capabilities for beam control in 2022 [161], as shown in Figure 9a. More related works on active metasurfaces with chalcogenides can be found in [170–172].

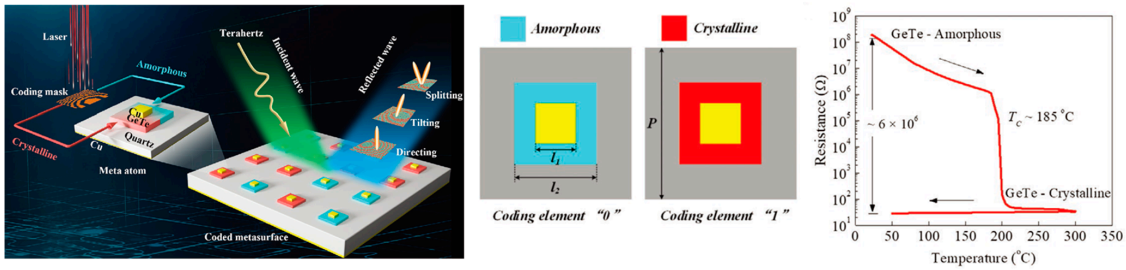

(**a**)

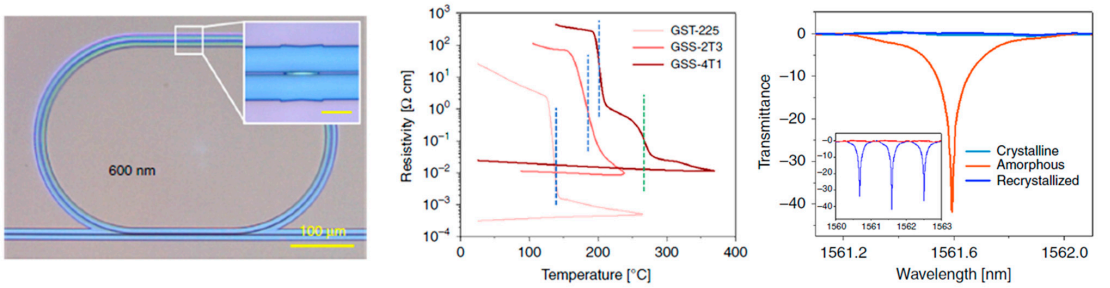

(**b**)

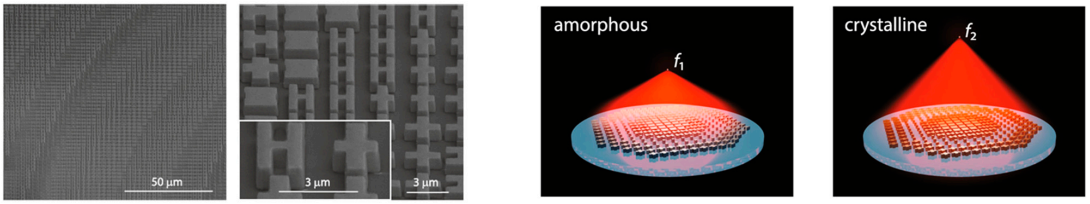

(**c**)

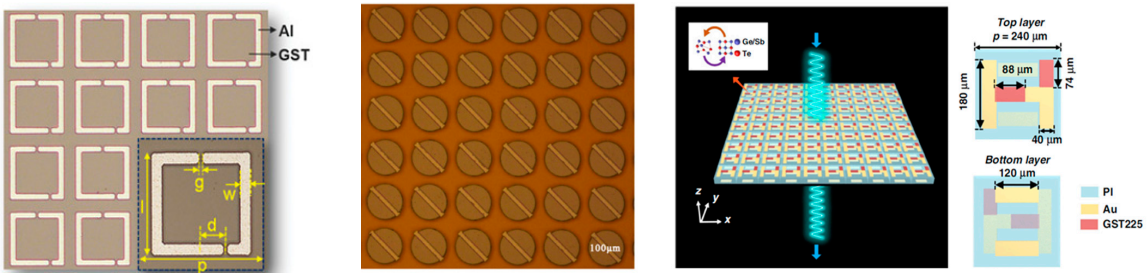

(**d**) (**e**) (**f**)

Figure 9. Chalcogenides and active metasurfaces with chalcogenides. (**a**) Programmable metasurfaces with GT [161]. The phase transition temperature is ~185°. Copyright John Wiley and Sons, 2022. (**b**) Reconfigurable optical resonator switch with $Ge_2Sb_2Se_4Te_1$ and temperature dependence of resistivity of $Ge_2Sb_2Te_5$, $Ge_2Sb_2Se_2Te_3$, and $Ge_2Sb_2Se_4Te_1$ [162]. (**c**) Reconfigurable all−dielectric metalens with diffraction−limited performance controlled by $Ge_2Sb_2Se_4Te_1$ [13]. (**d**) Active metasurfaces with $Ge_2Sb_2Te_5$ at terahertz frequencies [167]. Copyright John Wiley and Sons, 2019. (**e**) Broadband polarization converter with cut−wire metamaterials and $Ge_2Sb_2Te_5$ [168]. (**f**) Nonvolatile chiral metasurface switches with $Ge_2Sb_2Te_5$ [169].

As a kind of newly rising PCMs, chalcogenides meet many problems to be solved. Taking the well−studied $Ge_2Sb_2Te_5$ for instance, the optical constants and amorphous phase properties show considerable differences between different papers and various preparation

methods [163]. In addition, intermediate states comprising mixtures of amorphous and crystalline phases may be formed sensitively depending on the treatment conditions, which results in inconstant electrical and optical properties. The filamentation phenomenon may hamper uniform crystallization in the electrical bias method [173].

6. Conclusions and Prospects

This review represents a comprehensive summary of active and programmable metasurfaces from the aspect of semiconductor devices and materials, discusses the physical mechanisms, electrical circuits, device configurations, and recent developments, and shows the pros and cons of various approaches as well as their applications. Currently, state−of−the−art works have been done in multiple control devices with different stimuli, 3−D structures, non−reciprocal physics, low−dimensional active materials, and digital devices, which have found promising applications in RIS [5], holography [7], cloaking [10], and optical computing [9]. Active and programmable metasurfaces should be important technologies for the rising 6G communication, augmented reality, and artificial intelligence in the near future. It is beyond our capacity to cover all important works reported and foresee every new trend in the limited pages so that we will concentrate our prospects on the aforementioned contents in this review.

Currently, varactor and PIN diodes encounter significant frequency limits, which may be overcome by using new semiconductor materials with high mobility, small devices with a short electron transfer length, as well as new structures for similar functionalities, such as the MSM varactor with dual Schottky junctions [37]. Schottky diodes naturally have high working frequencies up to the terahertz range. However, the advanced Schottky diodes have considerable fabrication difficulties and, thus, may be too expensive for large array applications. Transistors including HEMTs and TFTs address high−frequency capabilities and high controllability. However, the additional gate electrode induces extra complexity for the design of metasurfaces and biasing networks. In addition, these high−frequency transistors are expensive for large metasurface arrays. Notably, most programmable metasurfaces with semiconductor devices are based on PCBs, which can provide multilayer circuits for the metasurfaces and bias networks. However, most of the PCB materials and commercial fabrication technologies cannot support terahertz applications due to the high−loss tangent and large manufacturing resolutions [174,175]. In this regard, PCB−compatible oxide semiconductors, such as IGZO [75–77], may find important applications in high−frequency programmable metasurfaces.

On the other hand, material uniformity, repeatability, and modulation consistency are important challenges for the newly rising semiconductor materials. Mechanically exfoliated graphene may exhibit a high electron mobility up to 200,000 $cm^2/(V \cdot s)$ [176,177]; however, the dimensions of which are typically less than tens of micrometers. Chemical vapor deposition (CVD) graphene has a large area with wrinkles, defects, and double−layer overlaps, whose electrical and optical properties are not as uniform as the exfoliated graphene. PCMs may achieve nanosecond modulation speed with electrical biasing. However, the crystallization in phase transition may be not uniform, and filamentation needs to be avoid in practical applications [162]. In addition, the bias networks for graphene and PCMs are not as powerful as that of the diode−based programmable metasurfaces, which significantly limits their RIS applications. Even so, graphene and PCMs are promising for the future active and programmable metasurfaces. We hope that more work will be reported to find good solutions in the near future.

Author Contributions: Conceptualization, Y.Z.; investigation, C.C., J.M., X.W., T.S., and K.C.; data curation, X.W., T.S., and K.C.; writing—original draft preparation, C.C., and J.M.; writing—review and editing, Y.Z., J.M., and X.Z.; visualization, C.C., X.W., T.S., and K.C.; project administration, Y.Z.; funding acquisition, Q.W. and Y.Z. All authors have read and agreed to the published version of the manuscript.

Funding: This research was funded by National Key Research and Development Program of China (2022YFA1405200); Key Research and Development Program of Shandong Province (2019JZZY020109); National Natural Science Foundation of China (61701283); China Postdoctoral Science Foundation funded project (2018T110689, 2017M622201); Postdoctoral Innovation Program of Shandong Province (20171006).

Data Availability Statement: Data available on request.

Acknowledgments: The authors would like to thank the Multidisciplinary Precision Oncology Project of Shandong University for supporting this work.

Conflicts of Interest: The authors declare no conflict of interest.

References

1. Schurig, D.; Mock, J.J.; Justice, B.J.; Cummer, S.A.; Pendry, J.B.; Starr, A.F.; Smith, D.R. Metamaterial electromagnetic cloak at microwave frequencies. *Science* **2006**, *314*, 977–980. [CrossRef]
2. Fan, J.X.; Zhang, L.; Wei, S.S.; Zhang, Z.; Choi, S.K.; Song, B.; Shi, Y.S. A review of additive manufacturing of metamaterials and developing trends. *Mater. Today* **2021**, *50*, 303–328. [CrossRef]
3. Kadic, M.; Milton, G.W.; van Hecke, M.; Wegener, M. 3D metamaterials. *Nat. Rev. Phys.* **2019**, *1*, 198–210. [CrossRef]
4. Bao, L.; Cui, T.J. Tunable, reconfigurable, and programmable metamaterials. *Microw. Opt. Technol. Lett.* **2020**, *62*, 9–32. [CrossRef]
5. Xiao, S.; Wang, T.; Liu, T.; Zhou, C.; Jiang, X.; Zhang, J. Active metamaterials and metadevices: A review. *J. Phys. D Appl. Phys.* **2020**, *53*, 503002. [CrossRef]
6. Ren, Y.; Zhang, J.J.; Gao, X.X.; Zheng, X.; Liu, X.Y.; Cui, T.J. Active spoof plasmonics: From design to applications. *J. Phys. Condens. Matter* **2021**, *34*, 053002. [CrossRef]
7. Padilla, W.J.; Averitt, R.D. Imaging with metamaterials. *Nat. Rev. Phys.* **2021**, *4*, 85–100. [CrossRef]
8. Walia, S.; Shah, C.M.; Gutruf, P.; Nili, H.; Chowdhury, D.R.; Withayachumnankul, W.; Bhaskaran, M.; Sriram, S. Flexible metasurfaces and metamaterials: A review of materials and fabrication processes at micro− and nano−scales. *Appl. Phys. Rev.* **2015**, *2*, 011303. [CrossRef]
9. Zangeneh−Nejad, F.; Sounas, D.L.; Alù, A.; Fleury, R. Analogue computing with metamaterials. *Nat. Rev. Mater.* **2020**, *6*, 207–225. [CrossRef]
10. Shalaginov, M.Y.; Campbell, S.D.; An, S.S.; Zhang, Y.F.; Ríos, C.; Whiting, E.B.; Wu, Y.H.; Kang, L.; Zheng, B.W.; Fowler, C.; et al. Design for quality: Reconfigurable flat optics based on active metasurfaces. *Nanophotonics* **2020**, *9*, 3505–3534. [CrossRef]
11. Zhang, X.G.; Jiang, W.X.; Jiang, H.L.; Wang, Q.; Tian, H.W.; Bai, L.; Luo, Z.J.; Sun, S.; Luo, Y.; Qiu, C.W.; et al. An optically driven digital metasurface for programming electromagnetic functions. *Nat. Electron.* **2020**, *43*, 165–171. [CrossRef]
12. Zhang, L.; Chen, M.Z.; Tang, W.; Dai, J.Y.; Miao, L.; Zhou, X.Y.; Jin, S.; Cheng, Q.; Cui, T.J. A wireless communication scheme based on space− and frequency−division multiplexing using digital metasurfaces. *Nat. Electron.* **2021**, *4*, 218–227. [CrossRef]
13. Shalaginov, M.Y.; An, S.S.; Zhang, Y.F.; Yang, F.; Su, P.; Liberman, V.; Chou, J.B.; Roberts, C.M.; Kang, M.; Ríos, C.; et al. Reconfigurable all−dielectric metalens with diffraction−limited performance. *Nat. Commun.* **2021**, *12*, 1225. [CrossRef]
14. Guo, X.X.; Ding, Y.M.; Duan, Y.; Ni, X.J. Nonreciprocal metasurface with space−time phase modulation. *Light Sci. Appl.* **2019**, *8*, 123. [CrossRef]
15. Taravati, S.; Eleftheriades, G.V. Full−duplex reflective beamsteering metasurface featuring magnetless nonreciprocal amplification. *Nat. Commun.* **2021**, *12*, 4414. [CrossRef]
16. Sobolewski, J.; Yashchyshyn, Y. State of the art sub−terahertz switching solutions. *IEEE Access* **2022**, *10*, 12983–12989. [CrossRef]
17. Wang, Z.M.; Qiao, J.; Zhao, S.Q.; Wang, S.L.; He, C.; Tao, X.T.; Wang, S.P. Recent progress in terahertz modulation using photonic structures based on two−dimensional materials. *InfoMat* **2021**, *3*, 1110–1133. [CrossRef]
18. Sze, S.M.; Ng, K.K. *Physics of Semiconductor Devices*, 3rd ed.; John Wiley & Sons, Inc.: Hoboken, NJ, USA, 2006; pp. 60–93.
19. Zhao, J.; Cheng, Q.; Chen, J.; Qi, M.Q.; Jiang, W.X.; Cui, T.J. A tunable metamaterial absorber using varactor diodes. *New J. Phys.* **2013**, *15*, 043049. [CrossRef]
20. Capolino, F. *Applications of Metamaterials*, 1st ed.; CRC Press: Boca Raton, FL, USA, 2017.
21. Fu, X.J.; Cui, T.J. Recent progress on metamaterials: From effective medium model to real−time information processing system. *Prog. Quant. Electron.* **2019**, *67*, 100223. [CrossRef]
22. Salim, A.; Lim, S. Review of recent metamaterial microfluidic sensors. *Sensors* **2018**, *18*, 232. [CrossRef]
23. Sievenpiper, D.; Schaffner, J. Beam steering microwave reflector based on electrically tunable impedance surface. *Electron. Lett.* **2002**, *38*, 1237–1238. [CrossRef]
24. Sievenpiper, D.F.; Schaffner, J.H.; Song, H.J.; Loo, R.Y.; Tangonan, G. Two−dimensional beam steering using an electrically tunable impedance surface. *IEEE Trans. Antennas Propag.* **2003**, *51*, 2713–2722. [CrossRef]
25. Mias, C.; Yap, J.H. A varactor−tunable high impedance surface with a resistive−lumped−element biasing grid. *IEEE Trans. Antennas Propag.* **2007**, *55*, 1955–1962. [CrossRef]
26. Kim, H.K.; Lee, D.; Lim, S. Frequency−tunable metamaterial absorber using a varactor−loaded fishnet−like resonator. *Appl. Opt.* **2016**, *55*, 4113–4118.

27. Ma, B.; Liu, S.; Kong, X.; Jiang, Y.; Xu, J.; Yang, H. A novel wide−band tunable metamaterial absorber based on varactor diode/graphene. *Optik* **2016**, *127*, 3039–3043. [CrossRef]
28. Guo, Q.X.; Li, Z.R.; Su, J.X.; Song, J.M.; Yang, L.Y. Active frequency selective surface with wide reconfigurable passband. *IEEE Access* **2019**, *7*, 38348–38355. [CrossRef]
29. Zhang, W.; Lin, J.H.; Fang, X.H.; Lin, Y.X.; Wang, K.; Zhang, M. An active electromagnetically induced transparency (EIT) metamaterial based on conductive coupling. *Materials* **2022**, *15*, 7371. [CrossRef]
30. Boardman, A.D.; Grimalsky, V.V.; Kivshar, Y.S.; Koshevaya, S.V.; Lapine, M.; Litchinitser, N.M.; Malnev, V.N.; Noginov, M.; Rapoport, Y.G.; Shalaev, V.M. Active and tunable metamaterials. *Laser Photonics Rev.* **2011**, *5*, 287–307. [CrossRef]
31. Watts, C.M.; Liu, X.L.; Padilla, W.J. Metamaterial electromagnetic wave absorbers. *Adv. Mater.* **2012**, *24*, OP98–OP120. [CrossRef]
32. Wang, Y.F.; Yin, J.C.; Yuan, G.S.; Dong, X.C.; Du, C.L. Tunable I−shaped metamaterial by loading varactor diode for reconfigurable antenna. *Appl. Phys. A* **2011**, *104*, 1243–1247. [CrossRef]
33. Cui, T.J.; Qi, M.Q.; Wan, X.; Zhao, J.; Cheng, Q. Coding metamaterials, digital metamaterials and programmable metamaterials. *Light Sci. Appl.* **2014**, *3*, e218. [CrossRef]
34. Li, Y.B.; Li, L.L.; Xu, B.B.; Wu, W.; Wu, R.Y.; Wan, X.; Cheng, Q.; Cui, T.J. Transmission−type 2−bit programmable metasurface for single−sensor and single−frequency microwave imaging. *Sci. Rep.* **2016**, *6*, 23731. [CrossRef]
35. Li, L.L.; Cui, T.J.; Ji, W.; Liu, S.; Ding, J.; Wan, X.; Li, Y.B.; Jiang, M.H.; Qiu, C.W.; Zhang, S. Electromagnetic reprogrammable coding−metasurface holograms. *Nat. Commun.* **2017**, *8*, 197. [CrossRef]
36. Zhang, L.; Chen, X.Q.; Liu, S.; Zhang, Q.; Zhao, J.; Dai, J.Y.; Bai, G.D.; Wan, X.; Cheng, Q.; Castaldi, G.; et al. Space−time−coding digital metasurfaces. *Nat. Commun.* **2018**, *9*, 4334. [CrossRef]
37. Nouman, M.T.; Kim, H.W.; Woo, J.M.; Jeong, M.; Hwang, J.H.; Ji, H.; Kim, D.; Jang, J.H. Terahertz modulator based on metamaterials integrated with metal−semiconductor−metal varactors. *Sci. Rep.* **2016**, *6*, 26452. [CrossRef]
38. Kleinman, D.A. The forward characteristic of the pin diode. *Bell Syst. Tech. J.* **1956**, *35*, 685–706. [CrossRef]
39. Li, L. Machine−learning reprogrammable metasurface imager. *Nat. Commun.* **2019**, *10*, 1028. [CrossRef]
40. Cui, T.J.; Liu, S.; Bai, G.D.; Ma, Q. Direct transmission of digital message via programmable coding metasurface. *Research* **2019**, *2019*, 2584509. [CrossRef]
41. Ali, Q.; Shahzad, W.; Ahmad, I.; Safiq, S.; Bin, X.; Abbas, S.M.; Sun, H. Recent developments and challenges on beam steering characteristics of reconfigurable transmitarray antennas. *Electronics* **2022**, *11*, 587. [CrossRef]
42. Chang, T.K.; Langley, R.J.; Parker, E.A. An active square loop frequency selective surface. *IEEE Microw. Guided Wave Lett.* **1993**, *3*, 387–388. [CrossRef]
43. Philips, B.; Park, E.A.; Langley, R.J. Active FSS in an experimental horn antenna switchable between two beamwidths. *Electron. Lett.* **1995**, *31*, 1–2. [CrossRef]
44. Chang, T.K.; Langley, R.J.; Parker, E.A. Active frequency−selective surfaces. *IEE Proc.* **1996**, *143*, 62–66. [CrossRef]
45. Tanant, A.; Chambers, B. Experimental dual polarised phase−switched screen. *Electron. Lett.* **2003**, *39*, 119–121. [CrossRef]
46. Cahill, B.M.; Parker, E.A. Field switching in an enclosure with active FSS screen. *Electron. Lett.* **2001**, *37*, 244–245. [CrossRef]
47. Kiani, G.I.; Ford, K.L.; Esselle, K.P. Single−layer bandpass active frequency selective surface. Microw. *Opt. Technol. Lett.* **2008**, *50*, 2149–2151. [CrossRef]
48. Tennant, A.; Chambers, B. A single−layer tunable microwave absorber using an active FSS. *IEEE Microw. Wireless Compon. Lett.* **2004**, *14*, 46–47. [CrossRef]
49. Sanz−Izquierdo, B.; Parker, E.A.; Batchelor, J.C. Switchable frequency selective slot arrays. *IEEE Trans. Antennas Propag.* **2011**, *59*, 2728–2731. [CrossRef]
50. Chang, K.; Kwak, S.I. Active frequency selective surfaces using incorporated PIN diodes. *IECEI Trans. Electron.* **2008**, *91*, 1917–1922. [CrossRef]
51. Katko, A.R.; Hawkes, A.M. RF limiter metamaterial using p−i−n diodes. *IEEE Antennas Wirel. Propag. Lett.* **2011**, *10*, 1571–1573. [CrossRef]
52. Fan, Y.; Qiao, T. An electromagnetic modulator based on electrically controllable metamaterial analogue to electromagnetically induced transparency. *Sci. Rep.* **2017**, *7*, 40441. [CrossRef]
53. Li, Y.; Lin, J.; Guo, H.; Sun, W.; Xiao, S.; Zhou, L. A tunable metasurface with switchable functionalities: From perfect transparency to perfect absorption. *Adv. Optic. Mater.* **2020**, *8*, 1901548. [CrossRef]
54. Song, X.; Yang, W. Switchable metasurface for nearly perfect reflection, transmission, and absorption using PIN diodes. *Opt. Express.* **2021**, *29*, 29320–29328. [CrossRef]
55. Fang, J.; Huang, J. Research on broadband tunable metamaterial absorber based on PIN diode. *Optik* **2020**, *200*, 163171. [CrossRef]
56. Wu, Z.; Zhao, J. An active metamaterial absorber with ultrawideband continuous tunability. *IEEE Access* **2022**, *10*, 25290–25295. [CrossRef]
57. Tian, J.H.; Cao, X.Y.; Gao, J.; Yang, H.H.; Han, J.F.; Yu, H.C.; Wang, S.M.; Jin, R.; Li, T. A reconfigurable ultra−wideband polarization converter based on metasurface incorporated with PIN diodes. *J. Appl. Phys.* **2019**, *125*, 135105. [CrossRef]
58. Sumathi, K.; Lavadiya, S.; Yin, P.; Parmar, J.; Patel, S.K. High gain multiband and frequency reconfigurable metamaterial superstrate microstrip patch antenna for C/X/Ku−band wireless network applications. *Wirel. Netw.* **2021**, *27*, 2131–2146. [CrossRef]

59. Kumar, S.R.; Mithilesh, K. A metamaterial loaded hybrid fractal multiband antenna for wireless applications with frequency band reconfigurability characteristics. *Frequenz* **2020**, *74*, 401–416.
60. Al, G.M.; Muhammad, I. A Novel Design Reconfigurable Antenna Based on the Metamaterial for Wearable Applications. *J. Phys. Conf. Ser.* **2021**, *1973*, 012042.
61. Bao, L.; Ma, Q.; Wu, R.Y.; Fu, X.J.; Wu, J.W.; Cui, T.J. Programmable Reflection−Transmission Shared−Aperture Metasurface for Real−Time Control of Electromagnetic Waves in Full Space. *Adv. Sci.* **2021**, *8*, 2100149. [CrossRef]
62. Singh, A.; Mandal, M.K. Parasitic Compensation and Hence Isolation Improvement of PIN Diode Based Switches. *IEEE Trans. Circuits Syst. II* **2020**, *68*, 97–101. [CrossRef]
63. Liu, L.; Li, C.Y.; Zhang, Q.L.; Sun, X.W.; Sun, H. Design and analysis of a heterojunction AlGaAs/GaAs PIN diode structure. *Laser Optoelectron. Prog.* **2020**, *57*, 231604. [CrossRef]
64. Al-Ahmadi, N.A. Metal oxide semiconductor−based Schottky diodes: A review of recent advances. *Mater. Res. Express.* **2020**, *7*, 032001.
65. Harima, Y.; Okazaki, H.; Kunugi, Y. Formation of Schottky barriers at interfaces between metals and molecular semiconductors of p− and n−type conductances. *Appl. Phys. Lett.* **1996**, *69*, 1059–1061. [CrossRef]
66. Schlecht, M.T.; Preu, S. An efficient terahertz rectifier on the graphene/SiC materials platform. *Sci. Rep.* **2019**, *9*, 11205. [CrossRef]
67. Yang, F.; Meng, H.F.; Duo, W.B.; Sun, Z.L. Terahertz sub−harmonic mixer using discrete Schottky diode for planetary science and remote sensing. *Infrared Millim. Terahertz Waves* **2017**, *38*, 630–637. [CrossRef]
68. Bulcha, B.T.; Hesler, J.L.; Drakinskiy, V.; Stake, J.; Valavanis, A.; Dean, P.; Li, L.H.; Barker, N.S. Design and Characterization of 1.8–3.2 THz Schottky−Based Harmonic Mixers. *IEEE Trans. THz. Sci. Technol.* **2016**, *6*, 737–746. [CrossRef]
69. Zhang, B.; Lv, X.L.; He, J.; Xing, D.; Fan, Y.; Chen, X.D. 1.1 THz tenth harmonic mixer based on planar GaAs Schottky diode. *IET Microw. Antenna. Propag.* **2019**, *13*, 1799–1803. [CrossRef]
70. Liu, X.Y.; Zhang, Y.; Wang, H.R.; Wu, C.K.; Wei, H.M.; Xu, Y.H.; Zhou, J.T.; Jin, Z.; Yan, B. InGaAs/InP Schottky barrier diode with submicron T−shaped contact and Cut−Off frequency above 9 THz. *Infrared Phys. Techn.* **2022**, *123*, 104173. [CrossRef]
71. Chen, H.−T.; Padilla, W.J. Active terahertz metamaterial devices. *Nature* **2006**, *444*, 597–600. [CrossRef]
72. Chen, H.−T.; Padilla, W.J. A metamaterial solid−state terahertz phase modulator. *Nature* **2009**, *3*, 148–152. [CrossRef]
73. Chen, H.−T.; Lu, H. Electronic control of extraordinary terahertz transmission through subwavelength metal hole arrays. *Opt. Express* **2008**, *16*, 7641–7648. [CrossRef]
74. Liu, X.; Chen, H. Ultrabroadband electrically controllable terahertz modulation based on GaAs Schottky diode structure. *APL Photon.* **2021**, *6*, 111301. [CrossRef]
75. Zhang, Y.; Ling, H.; Chen, P.; Qian, P.; Shi, Y.; Wang, Y.; Feng, Y.; Xin, Q.; Wang, Q.; Shi, S.; et al. Tunable surface plasmon polaritons with monolithic Schottky diodes. *ACS Appl. Electron. Mater.* **2019**, *1*, 2124–2129. [CrossRef]
76. Ling, H.; Zhang, B.; Feng, M.; Qian, P.; Wang, Y.; Wang, Q.; Zhang, Y.; Song, A. Multi frequency multi bit amplitude modulation of spoof surface plasmon polaritons by Schottky diode bridged interdigital SRRs. *Sci. Rep.* **2021**, *11*, 19181. [CrossRef]
77. Ling, H.; Qian, P.; Zhang, B.; Feng, M.; Wang, Y.; Zhang, X.; Wang, Q.; Zhang, Y.; Song, A. Active terahertz metamaterials electrically modulated by InGaZnO Schottky diodes. *Opt. Mater. Express* **2021**, *11*, 2966–2974. [CrossRef]
78. Ratanak, P.; Sungjoon, L. Design and analysis of active metamaterial modulated by RF power level. *Sci. Rep.* **2020**, *10*, 8703.
79. Vassos, E.; Churm, J.; Powell, J.; Viegas, C.; Alderman, B.; Feresidis, A. Air−bridged Schottky diodes for dynamically tunable millimeter−wave metamaterial phase shifters. *Sci. Rep.* **2021**, *11*, 5988. [CrossRef]
80. Zhou, Y.J.; Dai, L.H.; Li, Q.Y.; Xiao, Z.Y. Two−Way Fano resonance switch in plasmonic metamaterials. *Front. Phys.* **2020**, *8*, 576419. [CrossRef]
81. Zhang, B.; Ji, D.; Fang, D.; Liang, S.; Fan, Y.; Chen, X. A novel 220−GHz GaN diode on−chip tripler with high driven power. *IEEE Electron. Device Lett.* **2019**, *40*, 780–783. [CrossRef]
82. Zhang, L.; Liang, S.; Lv, Y.; Yang, D.; Fu, X.; Song, X.; Gu, G.; Xu, P.; Guo, Y.; Bu, A.; et al. High−power 300 GHz solid−state source chain based on GaN doublers. *IEEE Electron. Device Lett.* **2021**, *42*, 1588–1591. [CrossRef]
83. Giuseppe, D.G.; Mohammed, S.; Vinay, C.; Priyanka, M.; Jeanne, T.; Malek, Z.; Guillaume, D.; Mohammed, Z.; Yannick, R. GaN Schottky diode on sapphire substrate for THz frequency multiplier applications. *Micro Nanostruct.* **2022**, *164*, 107116.
84. Liao, S.Y. *Microwave Devices and Circuits*, 3rd ed.; Perntice−Hall, Inc.: Englewood Cliffs, NJ, USA, 1990; p. 07632.
85. Mei, X.; Yoshida, W.; Lange, M.; Lee, J.; Zou, J.; Liu, P.H.; Leong, K.; Zamora, A.; Padilla, J.; Sarkozy, S.; et al. First demonstration of amplification at 1 THz using 25−nm InP high electron mobility transistor process. *IEEE Electron. Device Lett.* **2015**, *36*, 327–329. [CrossRef]
86. Hosono, H. How we made the IGZO transistor. *Nat. Electron.* **2018**, *1*, 428. [CrossRef]
87. Shrekenhamer, D.; Rout, S.; Strikwerda, A.C.; Bingham, C.; Averitt, R.D.; Sonkusale, S.; Padilla, W.J. High speed terahertz modulation from metamaterials with embedded high electron mobility transistors. *Opt. Express* **2011**, *19*, 9968–9975. [CrossRef] [PubMed]
88. Li, A.; Kim, S.; Luo, Y.; Li, Y.B.; Long, J.; Sievenpiper, D.F. High−power transistor−based tunable and switchable metasurface absorber. *IEEE Trans. Microw. Theory Techn.* **2017**, *65*, 2810–2818. [CrossRef]
89. Zhang, Y.X.; Qiao, S.; Liang, S.X.; Wu, Z.H.; Yang, Z.Q.; Feng, Z.H.; Sun, H.; Zhou, Y.C.; Sun, L.L.; Chen, Z.; et al. Gbps terahertz external modulator based on a composite metamaterial with a double−channel heterostructure. *Nano. Lett.* **2015**, *15*, 3501–3506. [CrossRef]

90. Zhang, Y.X.; Zhao, Y.C.; Liang, S.X.; Zhang, B.; Wang, L.; Zhou, T.C.; Kou, W.; Lan, F.; Zeng, H.X.; Han, J.G.; et al. Large phase modulation of THz wave via an enhanced resonant active HEMT metasurface. *Nanophotonics* **2018**, *8*, 153–170. [CrossRef]
91. Pan, W.; Yang, L.; Ma, Y.; Xiao, H.; Liu, B. Design of a terahertz dual−channel modulator based on metamaterials. *Appl. Opt.* **2021**, *60*, 9519–9524. [CrossRef]
92. Ren, F.F.; Xu, W.Z.; Lu, H.; Ye, J.D.; Tan, H.H.; Jagadish, C. Dynamic control of THz waves through thin−film transistor metamaterials. *Proc. SPIE* **2015**, *9668*, 96680O.
93. Xu, W.Z.; Ren, F.F.; Ye, J.D.; Lu, H.; Liang, L.J.; Huang, X.M.; Liu, M.K.; Shadrivov, I.V.; Powell, D.A.; Yu, G.; et al. Electrically tunable terahertz metamaterials with embedded large−area transparent thin−film transistor arrays. *Sci. Rep.* **2016**, *6*, 23486. [CrossRef]
94. Escorcia Carranza, I.; Grant, J.P.; Gough, J.; Cumming, D. Terahertz metamaterial absorbers implemented in CMOS technology for imaging applications: Scaling to large format focal plane arrays. *IEEE J. Sel. Top. Quant. Electron.* **2017**, *23*, 4700508. [CrossRef]
95. Liu, Y.S.; Sun, T.; Wu, X.J.; Bai, Z.Y.; Sun, Y.; Li, H.L.; Zhang, H.Y.; Chen, K.L.; Ruan, C.J.; Sun, Y.Z.; et al. Active tunable THz metamaterial array implemented in CMOS technology. *J. Phys. D Appl. Phys.* **2021**, *54*, 085107. [CrossRef]
96. Zeng, B.B.; Huang, Z.Q.; Singh, A.; Yao, Y.; Azad, A.K.; Mohite, A.D.; Taylor, A.J.; Smith, D.R.; Chen, H.-T. Hybrid graphene metasurfaces for highspeed mid−infrared light modulation and single−pixel imaging. *Light Sci. Appl.* **2018**, *7*, 51. [CrossRef]
97. Lee, S.J.; Baek, S.J.; Kim, T.T.; Cho, H.J.; Lee, S.H.; Kang, J.H.; Min, B. Metamaterials for enhanced optical responses and their application to active control of terahertz waves. *Adv. Mater.* **2020**, *32*, 2000250. [CrossRef]
98. Zhang, J.; Li, Z.F.; Shao, L.D.; Zhu, W.R. Dynamical absorption manipulation in a graphene−based optically transparent and flexible metasurface. *Carbon* **2021**, *176*, 374–382. [CrossRef]
99. Sang, M.Y.; Shin, J.; Kim, K.; Jun Yu, K. Electronic and thermal properties of graphene and recent advances in graphene based electronics applications. *Nanomaterials* **2019**, *9*, 374. [CrossRef]
100. Wang, J.G.; Mu, X.J.; Sun, M.T. The thermal, electrical and thermoelectric properties of graphene nanomaterials. *Nanomaterials* **2019**, *9*, 218. [CrossRef]
101. Katzmarek, D.A.; Aiswarya, P.; Ziolkowski, R.W.; Iacopi, F. Review of graphene for the generation, manipulation, and detection of electromagnetic fields from microwave to terahertz. *2D Mater.* **2022**, *9*, 022002. [CrossRef]
102. Ren, J.K.; Stagi, L.; Innocenzi, P. Hydroxylated boron nitride materials: From structures to functional applications. *J. Mater. Sci.* **2020**, *56*, 4053–4079. [CrossRef]
103. Maksoud, M.I.A.A.; Bedir, A.G.; Bekhit, M.; Abouelela, M.M.; Fahim, R.A.; Awed, A.S.; Attia, S.Y.; Kassem, S.M.; Elkodous, M.A.; El−Sayyad, G.S.; et al. MoS2−based nanocomposites: Synthesis, structure, and applications in water remediation and energy storage: A review. *Environ. Chem. Lett.* **2021**, *19*, 3645–3681. [CrossRef]
104. Zhu, H.Y.; Gan, X.; McCreary, A.; Lv, R.; Lin, Z.; Terrones, M. Heteroatom doping of two−dimensional materials: From graphene to chalcogenides. *Nano Today* **2020**, *30*, 100829. [CrossRef]
105. Grigorenko, A.N.; Polini, M.; Novoselov, K.S. Graphene plasmonics. *Nat. Photonics* **2012**, *6*, 749–758. [CrossRef]
106. Kumar, P.; Kumar Singh, A.; Hussain, S.; Nam Hui, K.; San Hui, K.; Eom, J.; Jung, J.; Singh, J. Graphene: Synthesis, properties and application in transparent electronic devices. *Rev. Adv. Sci. Eng.* **2013**, *2*, 238–258. [CrossRef]
107. Low, T.; Avouris, P. Graphene plasmonics for terahertz to mid IR applications. *ACS Nano* **2014**, *8*, 1086–1101. [CrossRef] [PubMed]
108. Li, J.; Li, J.T.; Yang, Y.; Li, J.N.; Zhang, Y.T.; Wu, L.; Zhang, Z.; Yang, M.S.; Zheng, C.L.; Li, J.H.; et al. Metal−graphene hybrid active chiral metasurfaces for dynamic terahertz wavefront modulation and near field imaging. *Carbon* **2020**, *163*, 34–42. [CrossRef]
109. Sambit Kumar, G.; Santanu, D.; Somak, B. Transmittive−type triple−band linear to circular polarization conversion in THz region using graphene−based metasurface. *Opt. Commun.* **2021**, *480*, 126480.
110. Novoselov, K.S.; Geim, A.K.; Morozov, S.V. Electric field effect in atomically thin carbon films. *Science* **2004**, *306*, 666–669. [CrossRef]
111. Balci1, O.; Polat, E.O.; Kakenov, N.; Kocabas, C. Graphene−enabled electrically switchable radar−absorbing surfaces. *Nat. Commun.* **2015**, *6*, 6628. [CrossRef]
112. Liu, M.; Yin, X.; Ulin Avila, E. A graphene−based broadband optical modulator. *Nature* **2011**, *474*, 64–67. [CrossRef]
113. Ju, L.; Geng, B.S.; Horng, J.; Girit, C.; Martin, M.; Hao, Z.; Bechtel, H.A.; Liang, X.G.; Zettl, A.; Ron Shen, Y.; et al. Graphene plasmonics for tunable terahertz metamaterials. *Nat. Nanotechnol.* **2011**, *6*, 630–634. [CrossRef]
114. Lee, S.H.; Choi, M.; Kim, T.T.; Lee, S.; Liu, M.; Yin, X.B.; Choi, H.K.; Lee, S.S.; Choi, C.G.; Choi, S.Y.; et al. Switching terahertz waves with gate−controlled active graphene metamaterials. *Nat. Mater.* **2012**, *11*, 936–941. [CrossRef]
115. Feng, H.; Xu, Z.X.; Li, K.; Wang, M.; Xie, W.L.; Luo, Q.P.; Chen, B.Y.; Kong, W.J.; Yun, M.J. Tunable polarization−independent and angle−insensitive broadband terahertz absorber with graphene metamaterials. *Opt. Express* **2021**, *29*, 7158–7167. [CrossRef]
116. Zhu, J.; Yin, J.G.; Wu, C.S. Tunable perfect absorber of graphene metamaterial in the terahertz band and its sensing properties. *Adv. Photonics Res.* **2022**, *3*, 2100291. [CrossRef]
117. Jiang, W.J.; Chen, T. A five−band absorber based on graphene metamaterial for terahertz ultrasensing. *Nanotechnology* **2022**, *33*, 165503. [CrossRef]
118. Liu, W.W.; Song, Z.Y. Terahertz absorption modulator with largely tunable bandwidth and intensity. *Carbon* **2020**, *174*, 617–624. [CrossRef]
119. Liu, Y.; Huang, R.; Ouyang, Z.B. Terahertz absorber with dynamically switchable dual−broadband based on a hybrid metamaterial with vanadium dioxide and graphene. *Opt. Express* **2021**, *29*, 20839–20850. [CrossRef]

120. Yao, H.Y.; Yan, X.; Yang, M.S.; Yang, Q.L.; Liu, Y.Y.; Li, A.Y.; Wang, M.; Wei, D.Q.; Tian, Z.J.; Liang, L.J. Frequency−dependent ultrasensitive terahertz dynamic modulation at the Dirac point on graphene−based metal and all−dielectric metamaterials. *Carbon.* **2021**, *184*, 400–408. [CrossRef]
121. Rajabalipanah, H.; Abdolali, A.; Rouhi, K. Reprogrammable spatiotemporally modulated graphene−based functional metasurfaces. *IEEE J. Emerg. Sel. Top. Circuits Syst.* **2020**, *10*, 75–87. [CrossRef]
122. Norouzi Razani, A.; Rezaei, P. Multiband polarization insensitive and tunable terahertz metamaterial perfect absorber based on the heterogeneous structure of graphene. *Opt. Quant. Electron.* **2022**, *54*, 407. [CrossRef]
123. Feng, M.M.; Zhang, B.Q.; Ling, H.T.; Zhang, Z.H.; Wang, Y.M.; Wang, Y.L.; Zhang, X.J.; Hua, P.R.; Wang, Q.P.; Song, A.M.; et al. Active metal–graphene hybrid terahertz surface plasmon polaritons. *Nanophotonis* **2022**, *11*, 3331–3338. [CrossRef]
124. Liu, P.Q.; Luxmoore, I.J.; Mikhailov, S.A.; Savostianova, N.A.; Valmorra, F.; Faist, J.; Nash, G.R. Highly tunable hybrid metamaterials employing split−ring resonators strongly coupled to graphene surface plasmons. *Nat. Commun.* **2015**, *6*, 8969. [CrossRef] [PubMed]
125. Choi, G.; Chau, T.K.; Hong, S.J.; Kim, D.; Kim, S.H.; Kim, D.S.; Suh, D.; Bahk, Y.M.; Jeong, M.S. Augmented all−optical active terahertz device using graphene−based metasurface. *Adv. Opt. Mater.* **2021**, *9*, 2100462. [CrossRef]
126. Efazat, S.S.; Raheleh Basiri, R.; Al−Din Makki, S.V. The gain enhancement of a graphene loaded reconfigurable antenna with non−uniform metasurface in terahertz band. *Optik* **2019**, *183*, 1179–1190. [CrossRef]
127. Shubham, A.; Samantaray, D.; Ghosh, S.K.; Dwivedi, S.; Bhattacharyya, S. Performance improvement of a graphene patch antenna using metasurface for THz applications. *Optik* **2022**, *264*, 169412. [CrossRef]
128. Jarchi, S. Radiation pattern direction control of THz antenna with applying planar graphene metasurface. *Optik* **2021**, *243*, 167458. [CrossRef]
129. Yanbin Luo, Y.B.; Zeng, Q.S.; Yan, X. A graphene−based tunable negative refractive index metamaterial and its application in dynamic beam−tilting terahertz antenna. *Microw. Opt. Technol. Lett.* **2019**, *61*, 2766–2772.
130. Gong, Y.M.; Hu, F.R.; Jiang, M.Z.; Zhang, L.H.; Zou, Y.C.; Jiang, G.B.; Liu, Y.C. Terahertz binary coder based on graphene metasurface. *Carbon* **2021**, *184*, 167–176. [CrossRef]
131. Leong, W.S.; Wang, H.; Yeo, J.; Martin−Martinez, F.J.; Zubair, A. Paraffin−enabled graphene transfer. *Nat. Commun.* **2019**, *10*, 867. [CrossRef]
132. Riffat, S.; Mempouo, B.; Fang, W. Phase change material developments: A review. *Int. J. Ambient Energy* **2013**, *36*, 102–115. [CrossRef]
133. Gonzalez−Hernandez, J.; Prokhorov, E.; Vorobiev, Y. Temperature dependence of structure and electrical properties of germanium−antimony−tellurium thin films. *J. Vac. Sci. Technol.* **2000**, *18*, 1694–1700. [CrossRef]
134. Zhu, H.Q.; Li, Y.; Li, Y.M.; Huang, Y.Z.; Tong, G.X.; Fang, B.Y.; Zheng, Q.X.; Li, L.; Shen, Y. Effect of annealing on optical properties and structure of the vanadium dioxide thin films. *Proc. SPIE* **2012**, *8418*, 84181S.
135. Inglesfield, J.E. The structure and phase changes of gallium. *J. Phys. C Solid State Phys.* **1968**, *1*, 1337. [CrossRef]
136. Jeong, Y.G.; Bahk, Y.M.; Kim, D.S. Dynamic terahertz plasmonics enabled by phase−change materials. *Adv. Opt. Mater.* **2019**, *8*, 1900548. [CrossRef]
137. Mou, N.L.; Tang, B.; Li, J.Z.; Zhang, Y.Q.; Dong, H.X.; Zhang, L. Demonstration of thermally tunable multi−Band and ultra−broadband metamaterial absorbers maintaining high efficiency during tuning process. *Materials* **2021**, *14*, 5708. [CrossRef]
138. Zhang, C.; Zhou, G.; Wu, J. Active control of terahertz waves using vanadium−dioxide−embedded metamaterials. *Phys. Rev. Appl.* **2019**, *11*, 054016. [CrossRef]
139. Dong, K.; Hong, S.; Deng, Y.; Ma, H.; Li, J.; Wang, X.; Yeo, J.; Wang, L.; Lou, S.; Tom, K.B.; et al. A lithography−free and field−programmable photonic metacanvas. *Adv. Mater.* **2018**, *30*, 1703878. [CrossRef]
140. Seo, M.; Kyoung, J.; Park, H.; Koo, S.; Kim, H.S.; Bernien, H.; Kim, B.J.; Choe, J.H.; Ahn, Y.H.; Kim, H.T.; et al. Active terahertz nanoantennas based on VO_2 phase transition. *Nano Lett.* **2010**, *10*, 2064–2068. [CrossRef]
141. Jeong, Y.G.; Han, S.; Rhie, J.; Kyoung, J.S.; Choi, J.W.; Park, N.; Hong, S.; Kim, B.-J.; Kim, H.-T.; Kim, D.-S. A vanadium dioxide metamaterial disengaged from insulator−to−metal transition. *Nano Lett.* **2015**, *15*, 6318–6323. [CrossRef]
142. Wang, D.C.; Zhang, L.C.; Gu, Y.H.; Mehmood, M.Q.; Gong, Y.D.; Srivastava, A.; Jian, L.K.; Venkatesan, T.; Qiu, C.W.; Hong, M.H. Switchable ultrathin quarter−wave plate in terahertz using active phase−change metasurface. *Sci. Rep.* **2015**, *5*, 15020. [CrossRef]
143. Wang, S.X.; Kang, L.; Werner, D.H. Active terahertz chiral metamaterials based on phase transition of vanadium dioxide (VO_2). *Sci. Rep.* **2018**, *8*, 189. [CrossRef]
144. Jeong, Y.G.; Bernien, H.; Kyoung, J.-S.; Park, H.-R.; Kim, H.-S.; Choi, J.-W.; Kim, B.-J.; Kim, H.-T.; Ahn, K.J.; Kim, D.-S. Electrical control of terahertz nano antennas on VO_2 thin film. *Opt. Express* **2011**, *19*, 21211–21215. [CrossRef] [PubMed]
145. Vitale, W.A.; Tamagnone, M.; Emond, N.; Le Drogoff, B.; Capdevila, S.; Skrivervik, A.; Chaker, M.; Mosig, J.R.; Ionescu, A.M. Modulated scattering technique in the terahertz domain enabled by current actuated vanadium dioxide switches. *Sci. Rep.* **2017**, *7*, 41546. [CrossRef] [PubMed]
146. Kang, T.; Ma, Z.; Qin, J.; Peng, Z.; Yang, W.; Huang, T.; Xian, S.; Xia, S.; Yan, W.; Yang, Y.; et al. Large−scale, power−efficient Au/VO_2 active metasurfaces for ultrafast optical modulation. *Nanophotonics* **2020**, *10*, 909–918. [CrossRef]
147. Lu, X.G.; Dong, B.W.; Zhu, H.F.; Shi, Q.W.; Tang, L.; Su, Y.D.; Zhang, C.; Huang, W.X.; Cheng, Q. Two−channel VO_2 memory meta−device for terahertz waves. *Nanomaterials* **2021**, *11*, 3409. [CrossRef]

148. Luo, H.; Liu, H.; Chen, C.; Feng, Y.; Gao, P.; Ren, Z.Y.; Qiao, Y.J. Dual−broadband terahertz absorber based on phase transition characteristics of VO_2. *Results Phys.* **2022**, *34*, 105270. [CrossRef]
149. Li, Z.; Xia, H.; Zhao, Y.F.; Lei, W.T.; Zhao, C.Y.; Xie, W.K. Polarization−insensitive and absorption−tunable ultra−broadband terahertz metamaterial absorbers based on multiple resonant rings. *Results Phys.* **2022**, *39*, 105786. [CrossRef]
150. Song, Z.Y.; Zhang, J.H. Achieving broadband absorption and polarization conversion with a vanadium dioxide metasurface in the same terahertz frequencies. *Opt. Express* **2020**, *28*, 12487–12497. [CrossRef]
151. Shin, J.H.; Park, K.H.; Ryu, H.C. A band−switchable and tunable THz metamaterial based on an etched vanadium dioxide thin film. *Photonics* **2022**, *9*, 89. [CrossRef]
152. Sun, Z.S.; Wang, X.; Wang, J.L.; Li, H.; Lu, Y.H.; Zhang, Y. Switchable multifunctional terahertz metamaterials based on the phase−transition properties of vanadium dioxide. *Micromachines* **2022**, *13*, 1013. [CrossRef]
153. Liu, X.B.; Wang, Q.; Zhang, X.Q.; Li, H.; Xu, Q.; Xu, Y.H.; Chen, X.Y.; Li, S.X.; Liu, M.; Tian, Z.; et al. Thermally dependent dynamic meta−holography using a vanadium dioxide integrated metasurface. *Adv. Opt. Mater.* **2019**, *7*, 1900175. [CrossRef]
154. Du, H.T.; Jiang, M.Z.; Zeng, L.Z.; Zhang, L.H.; Xu, W.L.; Zhang, X.W.; Hu, F.R. Switchable terahertz polarization converter based on VO_2 metamaterial. *Chin. Phys. B* **2022**, *31*, 064210. [CrossRef]
155. Yang, C.H.; Gao, Q.G.; Dai, L.L.; Zhang, Y.L.; Zhang, H.Y.; Zhang, Y.P. Bifunctional tunable terahertz circular polarization converter based on Dirac semimetals and vanadium dioxide. *Opt. Mater. Express* **2020**, *10*, 2289–2303. [CrossRef]
156. Lv, F.; Wang, L.; Xiao, Z.Y.; Chen, M.M.; Cui, Z.T.; Xu, Q.D. Asymmetric transmission polarization conversion of chiral metamaterials with controllable switches based on VO_2. *Opt. Mater.* **2021**, *114*, 110667. [CrossRef]
157. Hu, F.R.; Wang, H.; Zhang, X.W.; Xu, X.L.; Jiang, W.Y.; Rong, Q.; Zhao, S.; Jiang, M.Z.; Zhang, W.T.; Han, J.G. Electrically triggered tunable terahertz band−pass filter based on VO_2 hybrid metamaterial. *IEEE J. Sel. Top. Quantum Electron.* **2019**, *25*, 4700207. [CrossRef]
158. Shabanpour, J. Programmable anisotropic digital metasurface for independent manipulation of dual−polarized THz waves based on a voltage−controlled phase transition of VO_2 microwires. *J. Mater. Chem. C* **2020**, *8*, 7189–7199. [CrossRef]
159. Li, Z.L.; Wang, W.; Deng, S.X.; Qu, J.; Li, Y.X.; Lv, B.; Li, W.J.; Gao, X.; Zhu, Z.; Guan, C.Y.; et al. Active beam manipulation and convolution operation in VO(2)−integrated coding terahertz metasurfaces. *Opt. Lett.* **2022**, *47*, 441–444. [CrossRef]
160. Li, J.; Yang, Y.; Li, J.N.; Zhang, Y.T.; Zhang, Z.; Zhao, H.L.; Li, F.Y.; Tang, T.T.; Dai, H.T.; Yao, J.Q. All−optical switchable vanadium dioxide integrated coding metasurfaces for wavefront and polarization manipulation of terahertz beams. *Adv. Theory Simul.* **2020**, *3*, 1900183. [CrossRef]
161. Lin, Q.W.; Wong, H.; Huitema, L.; Crunteanu, A. Coding metasurfaces with reconfiguration capabilities based on optical activation of phase−change materials for terahertz beam manipulations. *Adv. Opt. Mater.* **2022**, *10*, 2101699. [CrossRef]
162. Zhang, Y.F.; Chou, J.B.; Li, J.Y.; Li, H.S.; Du, Q.Y.; Yadav, A.; Zhou, S.; Shalaginov, M.Y.; Fang, Z.R.; Zhong, H.K.; et al. Broadband transparent optical phase change materials for high−performance nonvolatile photonics. *Nat. Commun.* **2019**, *10*, 4279. [CrossRef]
163. Zhang, Y.F.; Rios, C.; Shalaginov, M.Y.; Li, M.; Majumdar, A.; Gu, T.; Hu, J.J. Myths and truths about optical phase change materials: A perspective. *Appl. Phys. Lett.* **2021**, *118*, 210501. [CrossRef]
164. Wang, Q.; Rogers, E.T.F.; Gholipour, B.; Wang, C.-M.; Yuan, G.H.; Teng, J.H.; Zheludev, N.I. Optically reconfigurable metasurfaces and photonic devices based on phase change materials. *Nat. Photonics* **2016**, *10*, 60. [CrossRef]
165. Kodama, C.H.; Coutu, R.A. Coutu Tunable split−ring resonators using germanium telluride. *Appl. Phys. Lett.* **2016**, *108*, 231901. [CrossRef]
166. Gholipour, B.; Piccinotti, D.; Karvounis, A.; MacDonald, K.F.; Zheludev, N.I. Reconfigurable ultraviolet and high−energy−visible dielectric metamaterials. *Nano Lett.* **2019**, *19*, 1643–1648. [CrossRef] [PubMed]
167. Pitchappa, P.; Kumar, A.; Prakash, S.; Jani, H.; Venkatesan, T.; Singh, R. Chalcogenide phase change material for active terahertz photonics. *Adv. Mater.* **2019**, *31*, 1808157. [CrossRef]
168. Chen, J.J.; Chen, X.Y.; Liu, K.; Zhang, S.J.; Cao, T.; Tian, Z. A thermally switchable bifunctional metasurface for broadband polarization conversion and absorption based on phase−change material. *Adv. Photonics Res.* **2022**, *3*, 2100369. [CrossRef]
169. Bao, J.X.; Chen, X.Y.; Liu, K.; Zhan, Y.; Li, H.Y.; Zhang, S.J.; Xu, Y.H.; Tian, Z.; Cao, T. Nonvolatile chirality switching in terahertz chalcogenide metasurfaces. *Microsyst. Nanoeng.* **2022**, *8*, 112. [CrossRef]
170. Yang, F.; An, S.S.; Shalaginov, M.Y.; Zhang, H.L.; Rivero−Baleine, C.; Hu, J.J.; Gu, T. Design of broadband and wide−field−of−view metalenses. *Opt. Lett.* **2021**, *46*, 5735–5738. [CrossRef]
171. Guo, L.Y.; Ma, X.H.; Chang, Z.P.; Xu, C.L.; Jun, L.; Ran, Z. Tunable a temperature−dependent GST−based metamaterial absorber for switching and sensing applications. *J. Mater. Res. Technol.* **2021**, *14*, 772–779.
172. Xu, H.B. Design, simulation, and measurement of a multiband tunable metamaterial filter. *Opt. Mater.* **2022**, *127*, 112253.
173. Wuttig, M.; Bhaskaran, H.; Taubner, T. Phase−change materials for non−volatile photonic applications. *Nat. Photonics* **2017**, *11*, 465–476. [CrossRef]
174. Zhou, Z.; Li, W.; Qian, J.; Liu, W.; Wang, Y.; Zhang, X.; Guo, Q.; Yashchyshyn, Y.; Wang, Q.; Shi, Y.; et al. Flexible liquid crystal polymer technologies from microwave to Terahertz frequencies. *Molecules* **2022**, *27*, 1336. [CrossRef]
175. Wang, M.; Zhang, B.; Li, Z.; Wang, Y.; Guo, Q.; Liu, W.; Yashchyshyn, Y.; Song, A.; Zhang, Y. Frequency division multiplexer with directional filters in multilayer LCP films at E− and W−band. *IEEE Microw. Wireless Compon. Lett.* **2022**, *32*, 1287–1290. [CrossRef]

176. Auton, G.; But, D.B.; Zhang, J.; Hill, E.; Coquillat, D.; Consejo, C.; Nouvel, P.; Knap, W.; Varani, L.; Teppe, F.; et al. Terahertz detection and imaging using graphene ballistic rectifiers. *Nano Lett.* **2017**, *17*, 7015–7020. [CrossRef]
177. Auton, G.; Zhang, J.; Kumar, R.K.; Wang, H.; Zhang, X.; Wang, Q.; Hill, E.; Song, A. Graphene ballistic nano−rectifier with very high responsivity. *Nat. Commun.* **2016**, *7*, 11670. [CrossRef]

Disclaimer/Publisher's Note: The statements, opinions and data contained in all publications are solely those of the individual author(s) and contributor(s) and not of MDPI and/or the editor(s). MDPI and/or the editor(s) disclaim responsibility for any injury to people or property resulting from any ideas, methods, instructions or products referred to in the content.